remote sensing

MDPI

Article

Historical Mangrove Changes on Bangka Island Derived from Thirty Years of Landsat Data

Suci Puspita Sari [1,*], Nico Koedam [2,3,4,5], Tom Van der Stocken [6] and Frieke Van Coillie [7]

[1] Department of Marine Science, Universitas Bangka Belitung, Bangka 33172, Indonesia
[2] Systems Ecology and Resource Management, Department of Organism Biology, Université Libre de Bruxelles (ULB), Avenue F.D. Roosevelt 50, CPi 264/1, B1050 Brussels, Belgium; nikoedam@vub.be
[3] Marine Biology Research Group, Universiteit Gent, Krijgslaan 281–S8, B9000 Gent, Belgium
[4] Centre for Environmental Sciences (CMK), Universiteit Hasselt, Agoralaan z/n, B3590 Diepenbeek, Belgium
[5] Mangrove Specialist Group (MSG), Species Survival Commission (SSC), International Union for the Conservation of Nature (IUCN), 1196 Gland, Switzerland
[6] Ecology, Evolution & Genetics Research Group (bDIV), Department of Biology, Vrije Universiteit Brussel, Pleinlaan 2, B1050 Brussels, Belgium; tom.van.der.stocken@vub.be
[7] Q-ForestLab, Department of Environment, Ghent University, B9000 Ghent, Belgium; frieke.vancoillie@ugent.be
* Correspondence: sucipuspitasari@ubb.ac.id

Highlights

What are the main findings?

- Landsat-based random forest mapping and LandTrendr analysis (1994–2023) showed net mangrove loss on Bangka Island despite gains of ~4956.39 ha.
- Disturbance and recovery patterns varied strongly across the coast, linked to tin mining and accretion–erosion dynamics.

What are the implications of the main findings?

- Annual mangrove extent and change maps provide a practical baseline for monitoring and restoration prioritization in mining-impacted regions.
- Comparison with global mangrove datasets indicates that local validation is required to capture small or low-density stands omitted from global products.

Abstract

Bangka's mangroves contribute to Indonesia's species-rich coastal ecosystems, yet they have experienced substantial degradation, largely driven by human activities such as tin mining. Establishing long-term records of mangrove extent is essential for understanding distribution dynamics, assessing impacts, and guiding conservation strategies. In this study, we applied change detection techniques, a random forest classifier, and the LandTrendr algorithm to analyze Landsat time-series data from 1994 to 2023 across Bangka Island. We quantified multi-decadal changes in mangrove extent, periods of disturbance and recovery, and discrepancies between local and global datasets. Mangrove dynamics were spatially heterogeneous, with both expansion and loss observed across regions in landward and seaward settings. Over the 30-year period, total gains reached 4956.39 ha (10.30% of the baseline), yet the net change indicated an overall loss of 1055.85 ha. LandTrendr analysis further revealed sustained mangrove expansion since 1989. Observed changes reflect the combined influence of natural processes, including accretion and erosion, and human pressures, particularly tin mining. Although net area loss aligns with national trends, the drivers in this mining-dominated region differ from those elsewhere, and some mangrove areas remain absent from global datasets. These findings emphasize the need to better capture local gain–loss dynamics to support effective management and conservation.

Academic Editor: Chandra Giri

Received: 30 January 2026
Revised: 9 March 2026
Accepted: 13 March 2026
Published: 20 March 2026

Keywords: Bangka Island; Google Earth Engine; Landsat; LandTrendr; mangroves; mangrove index; spatiotemporal change; tin mining

1. Introduction

Mangroves are woody halophytes found within tropical, subtropical, and warm-temperate zones, generally between latitudes 30°N and 30°S [1,2]. These ecosystems flourish in intertidal zones, including deltas, estuaries, bays, lagoons, and oceanic atolls [3,4]. Mangroves support local fisheries, facilitate nutrient cycling, and sequester high amounts of carbon [5] for which they have been recognized as nature-based solutions in climate change mitigation [6,7]. Additionally, mangroves play an important role as natural barriers against coastal erosion, storm surges, and extreme weather, and contribute to enhancing water quality by trapping sediments and filtering pollutants [8,9].

Despite these ecosystem services, global-scale mangrove cover assessments indicate a net loss of 3.4% (5245 km^2) of mangrove extent from 1996 to 2020 [10]. Southeast Asia, which contains the largest mangrove area, has experienced the highest net loss, estimated at 2456.5 km^2 (4.8%), accounting for 47% of the global total mangrove loss [10]. Between 2000 and 2016, 62% of global mangrove losses were attributed to land-use changes, primarily aquaculture and agriculture, with nearly 80% of direct anthropogenic losses occurring in six countries: Indonesia, Myanmar, Malaysia, the Philippines, Thailand, and Vietnam [11]. Although global mangrove deforestation rates have generally decreased, ranging between 0.16% and 0.39% per year [12], countries like Myanmar and Malaysia continue to face high rates of loss, potentially increasing due to ambitious development plans [13].

Indonesia hosts the world's largest mangrove area and is among the most species-rich mangrove regions globally, with an estimated extent of 33,640 km^2 (3.36 million ha) in 2021 [14–16], representing about 24% of the global total [17]. The country supports approximately 46 of the 70 known mangrove species [1] and plays an important role in global climate change mitigation through its extensive mangrove carbon stocks [14]. However, Indonesia has experienced substantial mangrove loss, with about 261,141 ha degraded between 2009 and 2019, primarily due to deforestation (182,091 ha, or 70%) and ecosystem degradation (79,050 ha, or 30%) [17]. If this trend persists, Indonesia risks losing key mangrove functions within the next century, jeopardizing ecosystem services such as carbon sequestration [2]. Given that Indonesia harbors the largest mangrove area globally, conserving these carbon-rich forests is important for sustaining their contribution to global climate mitigation.

On Bangka Island in the Bangka Belitung Province, extensive mangrove loss has been driven by human activities, including the conversion of mangroves for shrimp ponds, settlements, and cumulative small-scale tin mining enterprises [10,18–21]. The island is included in the national mangrove restoration initiative under Presidential Decree No. 120 of 2020, which set a target to restore 600,000 ha of mangroves by 2024 to enhance community welfare. As part of this effort, the Ministry of Environment and Forestry (MoEF) implemented a labor-intensive mangrove planting program under the National Economic Recovery (PEN), targeting at least 500 ha in Bangka Selatan and Bangka Tengah regencies [22]. Despite these efforts, only about 100 ha of mangroves on Bangka Island have high restoration potential [23], highlighting the need for focused and well-planned strategies for long-term success. Tracking mangrove changes is essential to evaluate the effectiveness of restoration efforts, identify human and natural drivers, and assess their impacts [24]. However, monitoring mangrove dynamics remains challenging due to

persistent cloud cover, tidal dynamics, and limited access to historical optical satellite data in tropical regions, which constrain the accuracy of assessments [24,25].

Accurate and timely mangrove mapping is necessary to assess the extent and rate of loss before restoration plans are implemented, as well as to support policymaking, planning, and resource management [26]. Additionally, identifying areas of gain and loss informs the development and application of management and conservation strategies [27]. It also facilitates the estimation of primary production and carbon sequestration potential, aiding in determining areas suitable for protection or sustainable use [28].

Remote sensing has become an important approach for mapping mangrove ecosystems and monitoring their temporal dynamics because it enables consistent observation of coastal environments across large spatial extents and long time periods. In Southeast Asia, satellite imagery from the Landsat archive has been widely used to examine mangrove distribution and long-term changes in mangrove cover. For example, studies in Malaysia have applied Landsat time series analysis to assess mangrove regeneration and long-term dynamics of mangrove ecosystems [29–31]. In Indonesia, several studies have used Landsat imagery together with statistical and machine learning approaches, including decision tree and Random Forest classification, to map mangrove forests and analyze changes in mangrove extent [32–35]. Multi temporal Landsat observations have also been used to investigate mangrove disturbance, regeneration, and ecosystem dynamics in different coastal regions. These studies highlight the growing use of satellite time series analysis for understanding mangrove change and have contributed to the development of several regional and global mangrove mapping products.

Global mangrove mapping initiatives have employed a range of remote sensing imagery, analytical approaches, and temporal frameworks to characterize mangrove distribution and change [10,36–38]. These datasets have advanced understanding of global mangrove dynamics, supporting assessments of climate change impacts on mangrove extent and biomass [39], conservation status [40], and range shifts [41]. However, many global and regional mangrove datasets rely on bi-temporal or decadal analyses, which limits their ability to capture annual or interannual dynamics of mangrove change [24]. For example, the Global Mangrove Watch (GMW; [10]) maps mangrove extent for discrete periods (1996, 2007–2010, 2015–2020), providing long-term coverage but limited temporal resolution for capturing annual or interannual dynamics. Similarly, more recent datasets [38] focus on contemporary extent, emphasizing current distribution rather than changes over time.

Challenges in monitoring mangrove dynamics are further compounded at the national level, where mapping initiatives like the One-Map-Mangrove program and the Coastal Areas and Small Islands Zoning Plan (RZWP-3-K) often focus on specific time periods and are not publicly accessible. Limited long-term data on mangrove cover impedes accurate monitoring and trend assessment. Consequently, policymakers often lack reliable information on mangrove extent, and no continuous, province-level assessment exists for Bangka Island.

Previous studies on mangrove mapping in Bangka and nearby islands have generally been conducted at local scales or for limited observation periods [18,35,42–44]. These studies used various satellite sensors and analytical approaches, including Landsat-based NDVI analysis, ASTER imagery, and UAV observations to map mangrove extent or vegetation condition in specific locations. While these studies provide valuable insights into local mangrove conditions, most focus on individual sites or a small number of observation years, which limits the understanding of long-term mangrove dynamics across the entire island.

To address this gap, this study reconstructs a continuous annual mangrove extent dataset for Bangka Island from 1994 to 2023 using the Landsat archive within Google Earth Engine. By integrating multi-temporal satellite imagery, machine learning classification,

and time-series change detection, the study provides the first island-wide long-term assessment of mangrove dynamics on Bangka Island. The results reveal spatial patterns of mangrove gain and loss and identify periods of disturbance and recovery, providing information to support mangrove management and restoration planning in the region.

2. Materials and Methods

2.1. Study Area

The research area (Figures A1 and A2) covers the coastal mangrove ecosystems of Bangka Island, Indonesia. Bangka Island comprises four regencies (Bangka Barat, Bangka Tengah, Bangka Selatan, Bangka) and one city, Pangkalpinang, which serves as the provincial capital. Covering an area of approximately 12,000 km^2, Bangka Island is bordered by the Gaspar Strait to the east, the Bangka Strait to the west, the Java Sea to the south, and the Natuna Sea to the north [45]. The mangrove forests on this island represent approximately 70% of Indonesia's mangrove species [46,47].

Bangka Island is classified as having an equatorial fully humid (Af) climate according to the Köppen climate classification [48], with a dry season from June to October and a rainy season from October to May [49]. The island's average humidity is 82.3%, with an atmospheric pressure of 1007.9 millibars, and an average temperature of 28.2 °C. Annual rainfall is approximately 3012.9 mm, with 234 days of precipitation each year [45]. Situated within the Sunda Shelf/Java Sea ecoregion [26], Bangka Island is not impacted by tropical cyclones [50]. Hotspots of tropical cyclone- and sea-level-rise risk in Southeast Asia occur mainly in the Philippines, Vietnam, Malaysia, and only certain parts of Indonesia [51]. The tidal range varies between 2 m and 3 m, and over the last 25 years, sea level around Indonesia has risen at an average rate of 4.5 mm yr^{-1} [52,53].

2.2. Data

2.2.1. Landsat Images

Remote sensing analyses were performed using the Google Earth Engine (GEE) platform (https://code.earthengine.google.com/, accessed on 13 June 2024). The study area covered four Landsat World Reference System 2 (WRS-2) path/rows tiles: 122/61, 123/61, 123/62, and 124/61 (Figure A1). A total of 5083 Landsat surface reflectance (SR) Level 2, Collection 2, Tier 1 images were acquired for the period from 1994 to 2023. These datasets, available as image collections on GEE, comprise atmospherically corrected surface reflectance and land surface temperature products derived from the Landsat Thematic Mapper (TM), Enhanced Thematic Mapper Plus (ETM+), and Operational Land Imager/Thermal Infrared Sensor (OLI/TIRS) sensors (Table A1).

2.2.2. Data for Accuracy Assessment

The following global mangrove products were used for accuracy assessments: (1) Global Mangrove Forests Distribution (GMFD; [54]), (2) the Global Mangrove Watch v3.0 (GMW; [10]), and (3) High-resolution Global Mangrove Forests (HGMF_2020; [38]). The GMFD map, derived from Landsat 5 TM and Landsat 7 ETM+ data, employed a combination of supervised and unsupervised digital image classification techniques to map mangrove forests [54]. Because a globally consistent validation dataset was not available for this product, its evaluation relied mainly on comparisons with existing regional datasets and visual inspection using high-resolution satellite imagery available in Google Earth [54].

GMW utilized L-band Synthetic Aperture Radar (SAR) data from the Japan Aerospace Exploration Agency (JAXA) across 11 epochs (1996–2020), updating the baseline map (GMW v2.5) through a combination of thresholding techniques and a contextual mangrove change mask, thereby creating a detailed time series of mangrove extent changes [10]. The

GMW v3.0 dataset has been independently validated and reported an overall accuracy of about 93% for global mangrove extent mapping [10].

HGMF_2020 used object-based image analysis (OBIA) and random forest classification on Sentinel-2 composite images, allowing for high-resolution global mangrove mapping [38]. The dataset reported an overall accuracy of 95.2%, with user's accuracy and producer's accuracy for the mangrove class of 91.8% and 90.3%, respectively. Independent validation using bootstrapping further reported an overall accuracy of 93.6% (95% confidence interval: 91.4–95.7%). Mapping errors were mainly associated with confusion between mangrove forests and other coastal wetlands in some tropical regions [38]. In addition, sampling sites from ecological assessments [47] and Google Earth imagery were used as supporting reference data for validation.

2.3. Data Processing

The data processing workflow (Figure 1) includes pre-processing steps such as defining area of interest (AOI), cloud-free image composites generation, elevation masking, data filtering, AOI subsetting, spectral index computation, and training samples generation. This is followed by annual mangrove extent classification, accuracy assessment, change detection analysis, and LandTrendr analysis.

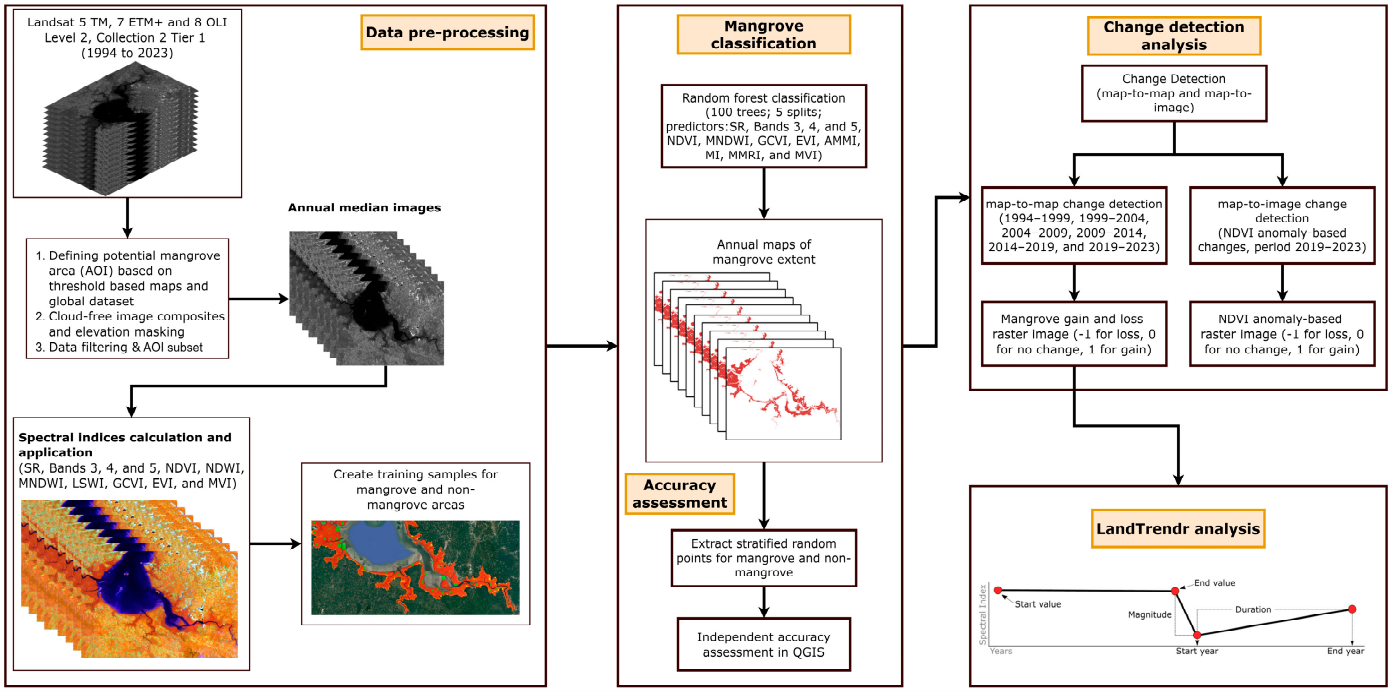

Figure 1. Flowchart of the methodology with an overview of the datasets used and the classification and change-detection process. The LandTrendr schematic is adapted from https://emapr.github.io/LT-GEE/imgs/segment_attributes.png, accessed on 13 June 2024.

2.3.1. Data Pre-Processing

1. Defining AOI

To ensure accurate analysis, AOI was defined using a combination of a coastline map of Bangka Island (https://tanahair.indonesia.go.id/portal-web/unduh, accessed on 13 June 2024), mangrove maps generated from rapid mapping using several mangrove indices, and global mangrove forest datasets. The coastline map served as the base layer to establish the coastal boundary, providing a geographical foundation for identifying potential mangrove areas. Mangrove maps from rapid mapping efforts were then overlaid with three global datasets—Global Mangrove Forest Distribution (GMFD; [54]), High-

resolution Global Mangrove Forests (HGMF_2020; [38]), and Global Mangrove Watch v3.0 (GMW; [10]), to compare and assess the spatial extent of mangroves.

Areas consistently identified as mangrove-covered across these datasets were prioritized, and any discrepancies between local and global data were carefully reviewed to refine the AOI boundaries. A 30 m buffer was applied to further extend the AOI, ensuring that areas where mangrove forests are likely to occur were included. It is worth noting that the buffer value was determined through numerous trials and errors to ensure that the AOI accurately encompassed the mangrove area.

2. Cloud-free image composites and elevation masking

Landsat datasets include a QA_PIXEL band, which contains pixel quality information derived from the CFMASK algorithm. This band is used to identify and exclude pixels affected by shadows, snow, or cloud cover, ensuring that only high-quality, cloud-free pixels are used in the analysis [55]. The cloud masking process for Landsat TM, ETM+, and OLI/TIRS sensors can be accessed through the following links: Landsat TM/ETM+ and Landsat OLI/TIRS.

To reduce image noise, the GEE median function was employed. The median composite was used to generate stable annual spectral representations of mangrove canopies by reducing residual cloud contamination, tidal variability, and extreme reflectance values that commonly occur in optical satellite imagery in tropical coastal environments. This function generates a composite image where each pixel value is the median of all unmasked pixels from the input stack for each band, resulting in noise-free median images devoid of extreme values [56]. Subsequently, median images were masked for the low-elevation coastal zone (LECZ), defined by elevations $\leq$ 40 m, which is a widely recognized criterion for delineating areas conducive to mangrove presence [57]. The elevation data for this study were sourced from Digital Elevation Model Nasiona (DEMNAS), which combines inputs from IFSAR, TERRASAR-X, and ALOS PALSAR, and is accessible through the Geospatial Information Agency website (https://tanahair.indonesia.go.id/portal-web/unduh, accessed on 13 June 2024), which provides high-resolution elevation data for accurately delineating the LECZ. The LECZ mask was used solely as a spatial constraint to exclude inland areas, rather than to represent the actual tidal elevation of mangroves.

3. Data filtering and AOI subset

Annual cloud-free image composites incorporating all visible and infrared bands were then generated for each observation year, covering the period from 1 January to 31 December, using Landsat (SR) Level 2, Collection 2, and Tier 1 data. These surface reflectance products are atmospherically corrected and designed to provide consistent reflectance measurements across Landsat sensors (TM, ETM+, and OLI/TIRS), enabling comparable spectral information to be used throughout the time series. To account for frequent cloud cover, the study period was extended by at least one year prior to the initial year, except when clear images were available (Table A2), assuming the mangrove area under clouds or shadows remained unchanged. When cloud-free observations were insufficient for a given year, imagery from up to two preceding years was included in the compositing process to ensure sufficient valid pixels for generating stable median composites. A spatial clipping operation was performed to define the precise AOI within the images before analysis.

4. Identification of potential mangrove areas/regions

Several spectral indices were applied to the annual cloud-free composite images for image masking and classification (Table A3). For masking, the following spectral indices were used: Enhanced Vegetation Index (EVI), Modified Normalized Difference Water Index (MNDWI), Normalized Difference Vegetation Index (NDVI), and Land Surface Water Index

(LSWI). Mangrove forests were identified using two main indicators: canopy cover (high leaf area index) and tidal inundation. Mangrove forest canopy coverage was determined using the thresholds NDVI > 0.3 and LSWI > 0.3. Tidal inundation was identified based on the condition LSWI $\geq$ EVI or LSWI $\geq$ NDVI [58] and MNDWI > -0.5. This step, combined with elevation masking, focused on identifying potential mangrove regions by selecting vegetated areas near water bodies and within suitable elevation ranges where mangroves are more likely to be found (Figure A3).

The images were then displayed using a false color composite (FCC), combining the Near-Infrared (NIR), Shortwave Infrared 1 (SWIR1), and Red bands (Table A4). This band combination enhances the visual distinction between vegetation and other land cover types, making it suitable for identifying mangrove and non-mangrove areas [59]. The FCC was used to delineate sampling areas based on distinct spectral and spatial patterns characteristic of mangroves and non-mangroves (e.g., built-up areas, water bodies, and bare land).

To ensure a comprehensive and representative sample, a total of 850 sampling areas were manually defined, comprising 500 mangrove and 350 non-mangrove areas, using visual interpretation and expert knowledge. The sampling polygons were distributed across the coastal zone within the AOI to capture the spatial variability of mangrove and non-mangrove land cover types in the study area. Because mangrove areas occupy a larger proportion of this zone, a larger number of samples were assigned to the mangrove class. Each sampling area was categorized as either mangrove or non-mangrove, with careful consideration of the spectral signatures and contextual information from the surrounding landscape. These sampling areas were used as training data for classification and further analysis. It is important to note that this sampling process was conducted exclusively for the initial observation year (1994), which serves as the reference classification image for subsequent analyses (Figure A4).

2.3.2. Mangrove Classification

Although Landsat satellites were launched in the 1970s, the earliest available image of Bangka Island dates back to 1989 and covers only a small portion of the island. To address these limitations, 1994 was chosen as the baseline year, as it offers complete coverage of the island with minimal cloud interference, providing high-quality data for more reliable analysis. During the pre-processing step (Section 2.3.1), sample areas for mangrove and non-mangrove regions were generated. Of these samples, 80% were allocated for training and 20% for testing, with the training set consisting of 56,263 pixels and the testing set consisting of 14,159 pixels.

A random forest classifier was then employed for classification, configured with 100 trees and 5 splits to balance performance and computational efficiency. Additional tests using a larger number of trees (200) produced similar validation accuracy, indicating that increasing the number of trees did not significantly improve classification performance. The approach used in this study follows the method described by Barenblitt and Fatoyinbo [60], with modifications to the predictors. Spectral features, including surface reflectance (SR), Bands 3, 4, and 5, and indices such as NDVI, MNDWI, Green Chlorophyll Vegeta-tion Index (GCVI), EVI, Automatic Mangrove Map and Index (AMMI), Mangrove Index (MI), Modular Mangrove Recog-nition Index (MMRI), and Mangrove Vegetation Index (MVI) (Table A3), were used as predictors for the model.

The classification process produced an annual binary map with two classes: 1 for mangrove area and 0 for non-mangrove area. To reduce noise in the classification images, connected pixels filtering was applied to eliminate isolated mangrove pixels [60]. This method effectively eliminates small, isolated pixel clusters that are less likely to

represent actual mangrove areas, thereby improving the overall classification accuracy. After training the random forest model on the 1994 dataset, it was applied to the annual image composites for each year from 1995 to 2023, producing annual mangrove extent maps. These predictors are derived from Landsat surface reflectance bands that are consistently available across TM, ETM+, and OLI/TIRS sensors, allowing the classification model trained using the 1994 dataset to be applied to subsequent years while maintaining comparable spectral information.

2.3.3. Accuracy Assessment

An independent accuracy assessment of the developed maps was conducted in QGIS software (v3.40.4 "Bratislava"; QGIS Development Team; https://qgis.org, accessed on 10 May 2024) using the Class Accuracy plugin. This process involved visual evaluation against available global mangrove datasets, Google Earth imagery, sampling sites from ecological assessment [47], and false color composites for each year. To evaluate classification accuracy, 150 stratified random samples were generated for each class (mangrove and non-mangrove) in every year, yielding 9000 samples across the 30-year period. Sample points were buffered by 15 m to account for resolution discrepancies, spatial misalignments, and edge effects between Landsat imagery and the reference data [60]. The evaluation involved generating a confusion matrix to derive overall accuracy (OA), producer accuracy (PA), and user accuracy (UA) metrics. This assessment was performed for annually produced mangrove maps. For additional validation, the developed mangrove maps were overlaid onto the respective Landsat scenes to visually assess their alignment.

2.3.4. Change Detection

Two approaches were employed for change detection: map-to-map and map-to-image using NDVI anomaly data according to the approaches described by Thomas et al. [61] and de Sousa et al. [62]. These two approaches were used to provide complementary perspectives on mangrove dynamics: the map-to-map method identifies categorical changes in mangrove extent, while the map-to-image approach evaluates changes in vegetation condition that may not yet appear as complete class transitions.

In the map-to-map approach, changes were identified by subtracting the mangrove extent map at year 1 (Y1) from the extent map at year 2 (Y2). To leverage the available 30-year dataset for a balanced assessment and effectively capture significant changes, seven periods of map-to-map change detection were performed at five-year intervals (1994–1999, 1999–2004, 2004–2009, 2009–2014, 2014–2019, and 2019–2023), as well as over a 30-year span (1994–2023). In the raster change analysis, pixels were categorized into three classes: -1 for mangrove loss, 0 for no change, and 1 for mangrove gain. Additionally, land cover in these regions was classified using a cloud-free composite image from 2023 to help identify the potential drivers of mangrove loss, supported by visual interpretation and comparison with high-resolution imagery available in Google Earth.

In contrast, the map-to-image approach used the 1994 baseline mangrove extent map to assess changes against a 2023 image, with change classes defined by specific threshold values. A change threshold of -0.2 was used to indicate significant mangrove loss, following a previously defined criterion [11]. This threshold reflects substantial decreases in NDVI values, which are typically associated with long-term or irreversible vegetation loss, such as deforestation or permanent land-use conversion. This method was selected due to minor but potentially significant differences in the spectral characteristics of the Landsat TM/ETM+ and OLI sensors, particularly in the near-infrared (NIR) and shortwave infrared (SWIR) bands, which are crucial for vegetation studies.

To account for these differences, the statistical transformations provided by Roy et al. [63] were applied to harmonize the spectral data between the TM/ETM+ and OLI/TIRS sensors, ensuring consistent spectral information and temporal continuity across datasets [62]. The harmonized Landsat TM/ETM+/OLI/TIRS collection was then used to derive NDVI anomaly-based changes in mangrove extent over the 30-year period from 1994 to 2023 on Bangka Island. In this context, an NDVI anomaly represents the difference between the NDVI value for a given time period and its long-term average. When the anomaly is close to zero, it indicates stable vegetation cover with no significant disturbances or changes. A positive NDVI anomaly indicates higher-than-average values, suggesting vegetation growth. Conversely, a negative anomaly reflects lower-than-average values, signaling potential vegetation loss or degradation [62].

2.3.5. LandTrendr Analysis

The map-to-map change detection results from 1994 and 2023, highlighting areas of mangrove loss and gain, were utilized to assess the timing of these changes (disturbance and recovery) using LandTrendr (Landsat-based Detection of Trends in Disturbance and Recovery), with Landsat observations beginning in 1984 to provide sufficient historical observations for identifying disturbance and recovery trajectories in the time-series analysis. NDVI was used as the primary spectral index to detect and track changes in mangrove area over time, as it effectively captures vegetation health and density. Areas identified as experiencing mangrove loss or gain were used as the focus for LandTrendr analysis, enabling the temporal assessment of when these changes occurred.

LandTrendr is a time-series analysis algorithm that tracks land cover changes over extended periods using Landsat satellite data. It segments satellite imagery into temporal change trends, enabling the identification of patterns such as deforestation, regrowth, or other shifts in land cover [64]. Although originally developed for forest disturbance monitoring, LandTrendr has also been applied to mangrove change analysis [24,65].

3. Results

3.1. Accuracy Assessment of Annual Mangrove Area Maps for Bangka Island

The mangrove area maps produced for each year of the study (1994–2023) demonstrate high accuracy, as evidenced by comparisons with global mangrove datasets and false-color composite images for each corresponding year. The overall accuracy (OA) ranges from 94% to 98.7%. Both producer accuracy (PA) and user accuracy (UA) are between 90% and 100% (Table A5). These results indicate that the classification accuracy remained consistently high across the 30-year time series.

3.2. Baseline Map and Spatial Distribution of Mangrove Forests on Bangka Island

A total of 48,120.88 ha of mangrove forest was classified in the baseline map of Bangka Island. There is no global mangrove dataset available for comparison with the 1994 baseline map, as the earliest dataset dates from 1996 [10]. The baseline map shows that mangroves on Bangka Island are concentrated around river mouths, small islands, and cover extensive areas in the northern and western parts. Additionally, a significant portion of these mangroves are located within protected and conserved zones, particularly in Bangka Barat and Bangka regencies (Figure 2).

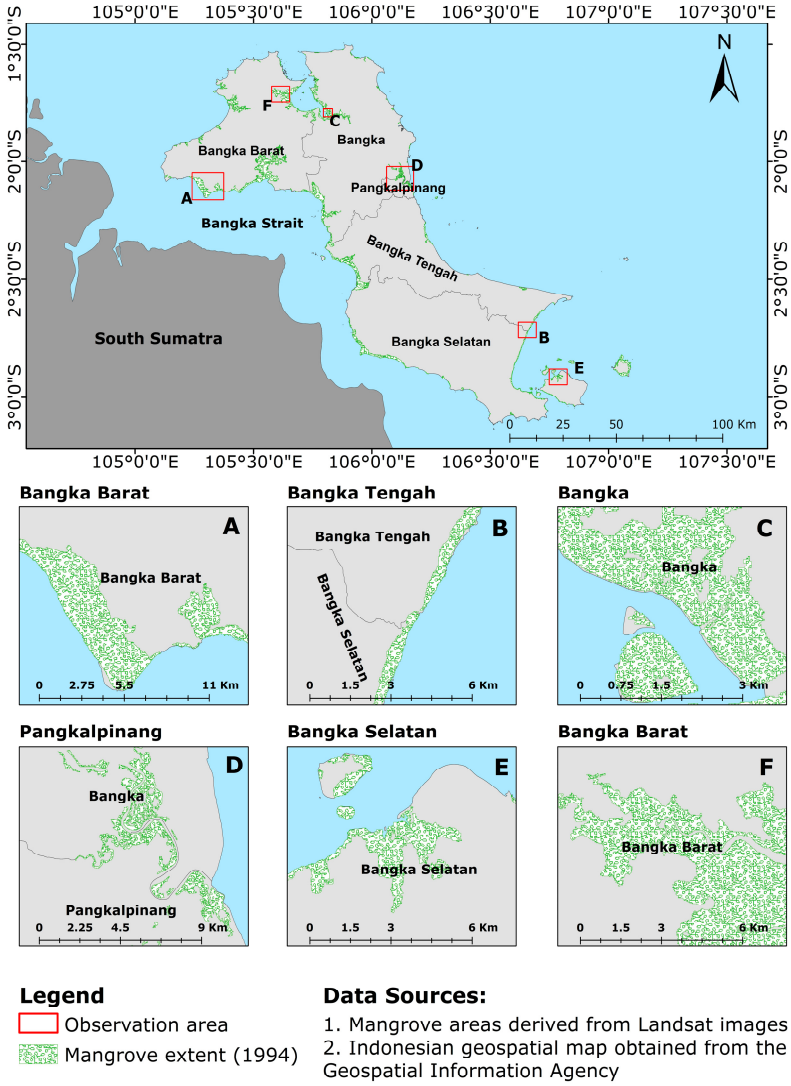

Figure 2. Baseline map of mangrove distribution on Bangka Island (1994). The map illustrates the spatial distribution of mangrove forests across Bangka Island, with notable concentrations in Bangka Barat, Bangka Tengah, Bangka, Bangka Selatan, and the city of Pangkalpinang. Red boxes (**A**–**F**) indicate selected observation areas used for detailed analysis.

3.3. Comparison of Annual Maps from Various Global Datasets

The classified extent successfully identified mangrove areas that were missing in most global datasets. Notably, there are significant differences in the total area of mangroves between the maps generated in this study and those from global datasets (Table 1 and Figure 3). For example, the total area of mangroves mapped in this study for 2015 was 17.53% greater than that reported by GMW v3 [10], with considerable discrepancies observed at specific sites such as Panjang Island in Bangka Tengah regency. The difference with GMFD [54] was smaller (2.86%), yet it still failed to capture areas such as Kayuanak Island in Bangka regency. The World Atlas of Mangroves (WAM) [4] dataset exhibited the largest discrepancy, with a 25.91% difference compared to the 2010 map from this study. The most recent dataset available at the time of analysis, HGMF_2020 [38], showed a 5.11% difference from the 2020 map in this study and did not include the small island of Seniur Island, which has been reported as a mangrove area in previous studies [47]. These discrepancies likely reflect differences in mapping methods, spatial filtering, and the observation years represented by each dataset. The visualization of annual mangrove maps, alongside global datasets, can be accessed through the following Google Earth En-

gine (GEE) apps: Mangrove Bangka Map 1 (https://sucipuspita1332.users.earthengine.app/view/mangrovebangka, accessed on 30 January 2026) and Mangrove Bangka Map 2 (https://sucipuspita1332.users.earthengine.app/view/mangrovebangka2, accessed on 30 January 2026) (Figures A8 and A9).

Table 1. Annual mangrove extent (ha) and comparison with selected global datasets.

Year	This Study	GMW v3	HGMF_2020	GMFD	WAM	Difference (%)
1994	48,120.88	–	–	–	–	–
1995	47,859.13	–	–	–	–	–
1996	48,062.04	40,981.37	–	–	–	17.28
1997	47,841.29	–	–	–	–	–
1998	47,776.57	–	–	–	–	–
1999	48,008.21	–	–	–	–	–
2000	48,188.39	–	–	46,850.63	–	2.86
2001	48,211.61	–	–	–	–	–
2002	47,623.71	–	–	–	–	–
2003	47,620.20	–	–	–	–	–
2004	47,650.14	–	–	–	–	–
2005	48,175.77	–	–	–	–	–
2006	47,800.56	–	–	–	–	–
2007	48,014.46	40,490.55	–	–	–	18.58
2008	47,686.81	40,286.81	–	–	–	18.37
2009	47,814.70	40,244.37	–	–	–	18.81
2010	48,147.23	40,438.49	–	–	38,238.12	19.06; 25.91
2011	47,602.48	–	–	–	–	–
2012	48,160.12	–	–	–	–	–
2013	48,569.56	–	–	–	–	–
2014	47,556.87	–	–	–	–	–
2015	47,456.81	40,379.15	–	–	–	17.53
2016	46,824.08	40,247.93	–	–	–	16.34
2017	46,495.22	40,157.53	–	–	–	15.78
2018	46,714.60	40,040.52	–	–	–	16.67
2019	47,484.93	39,819.68	–	–	–	19.25
2020	47,216.68	39,671.16	44,922.92	–	–	19.02; 5.11
2021	47,020.85	–	–	–	–	–
2022	47,119.84	–	–	–	–	–
2023	47,065.04	–	–	–	–	–

Note: GMW v3 = Global Mangrove Watch version 3; HGMF_2020 = High-resolution Global Mangrove Forests (2020); GMFD = Global Mangrove Forest Distribution; WAM = World Atlas of Mangroves.

3.4. Change Detection

3.4.1. Map-to-Map

Assessment of mangrove area change at five-year intervals (1994–1999, 1999–2004, 2004–2009, 2009–2014, 2014–2019, and 2019–2023) and over a 30-year period (1994–2023) reveals a general decline in mangrove area compared to the baseline map (Table 2 and Figure 4). Despite a gain of 4956.39 ha (10.30% of the baseline) over the 30-year period, the trend shows a decrease in mangrove extent, with a net loss of 1055.85 ha. This decline is uneven and varies across different regions, with specific areas showing distinct patterns of change. The only positive net change occurred during the period 2004–2009, when mangrove gain slightly exceeded mangrove loss (Table 2).

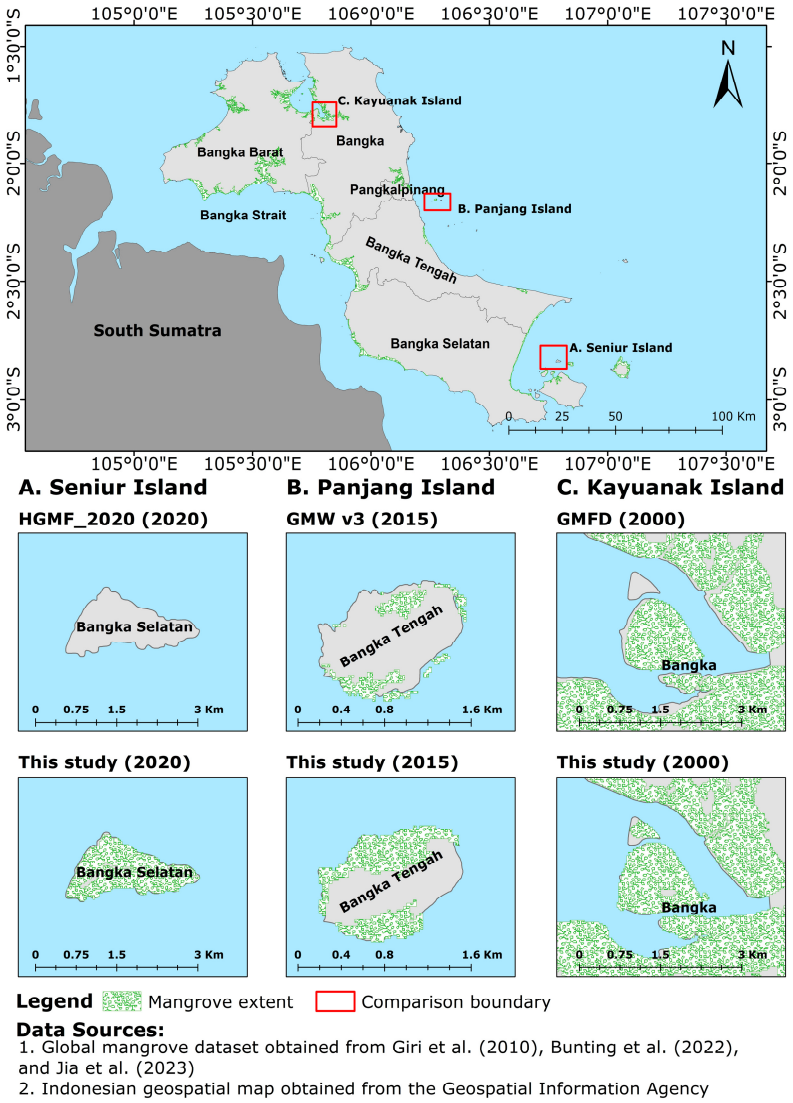

Figure 3. Comparison of mangrove extent between the baseline map generated in this study and selected global mangrove datasets for three selected comparison areas: (**A**) Seniur Island (2020), (**B**) Panjang Island (2015), and (**C**) Kayuanak Island (2000). Red boxes indicate the spatial boundaries used for comparison. For each site, the upper panels show global datasets (GMFD, GMW, and HGMF), while the lower panels show results from this study for the corresponding year [10,38,54].

Table 2. Mangrove gain and loss at five-year and 30-year intervals on Bangka Island.

Period	Net Change (ha)	Gain (ha)	Loss (ha)	Gain (%)	Loss (%)
1994–1999	↓ 112.67	3385.48	3498.15	7.04	7.27
1999–2004	↓ 358.07	2451.99	2810.06	5.11	5.85
2004–2009	↑ 164.56	2941.36	2776.79	6.17	5.83
2009–2014	↓ 257.83	2816.44	3074.27	5.89	6.43
2014–2019	↓ 71.94	2864.25	2936.19	6.02	6.17
2019–2023	↓ 419.90	2490.46	2910.35	5.24	6.13
1994–2023	↓ 1055.85	4956.39	6012.23	10.30	12.49

Note: ↓ (decreasing); ↑ (increasing).

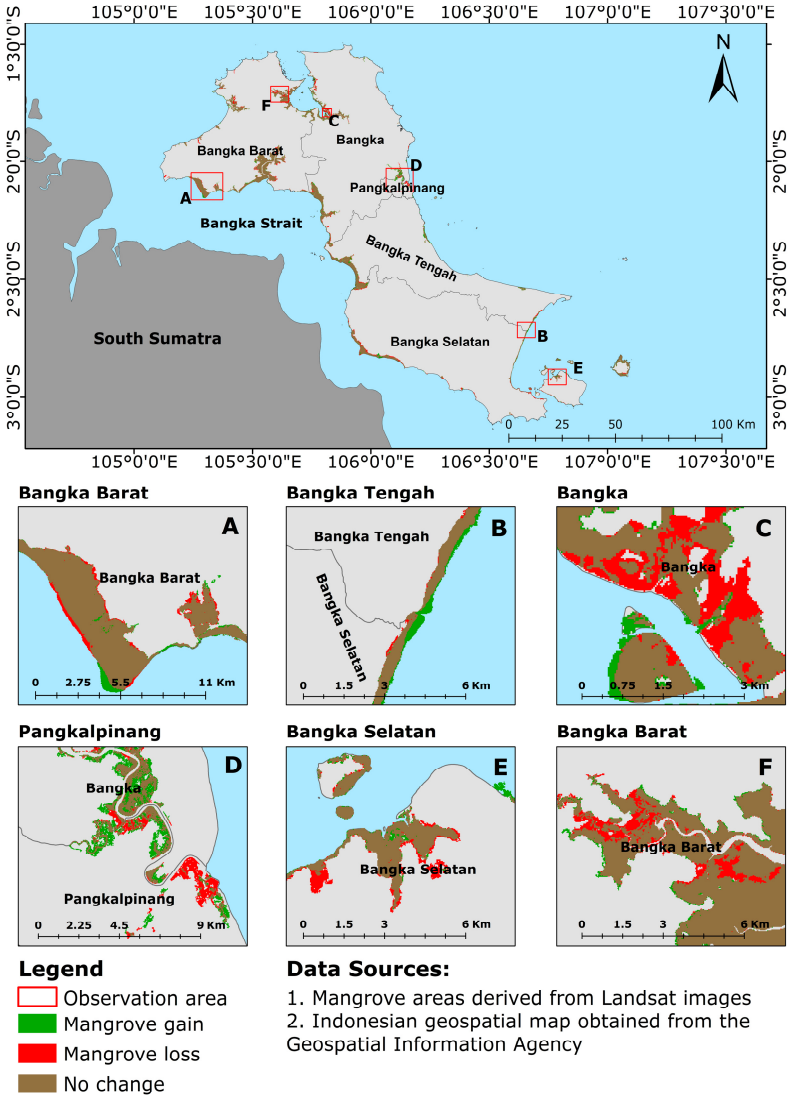

Figure 4. Mangrove gain, loss, and no change on Bangka Island over the 30-year study period. Island-wide patterns are shown in the main map, with panels (**A**–**F**) illustrating detailed changes within the selected observation areas.

The observed changes in mangrove area occur in both seaward and landward directions, reflecting both expansion and loss of mangrove areas. Drivers of mangrove loss include conversion to water bodies, non-mangrove vegetation, tin mining, bare land, and the development of aquaculture ponds (Table 3 and Figure 5). These land-use types were identified through visual interpretation of the 2023 Landsat composite and supporting high-resolution imagery available in Google Earth. For instance, in the Bangka Barat (Tanjung Punai) and Bangka Tengah regencies, mangrove expansion of approximately 500 m and 200 m, respectively, has been documented over the 30-year study period (Figure 4A,B). Conversely, in Bangka Barat regency, mangrove loss due to erosion has resulted in a ca. 200 m reduction (Figure 4A). Additionally, in Bangka regency, mangrove areas have decreased due to tin mining activities that have progressively expanded from the seaward to the landward side (Figure 4C).

Table 3. Drivers of mangrove loss over 30-year intervals (1994–2023) on Bangka Island.

Change	Area (ha)
Mangrove—Water body	2569.11
Mangrove—Non-mangrove	1811.57
Mangrove—Bare land	239.80
Mangrove—Aquaculture ponds	49.94
Mangrove—Mining area	1341.81
Total	**6012.23**

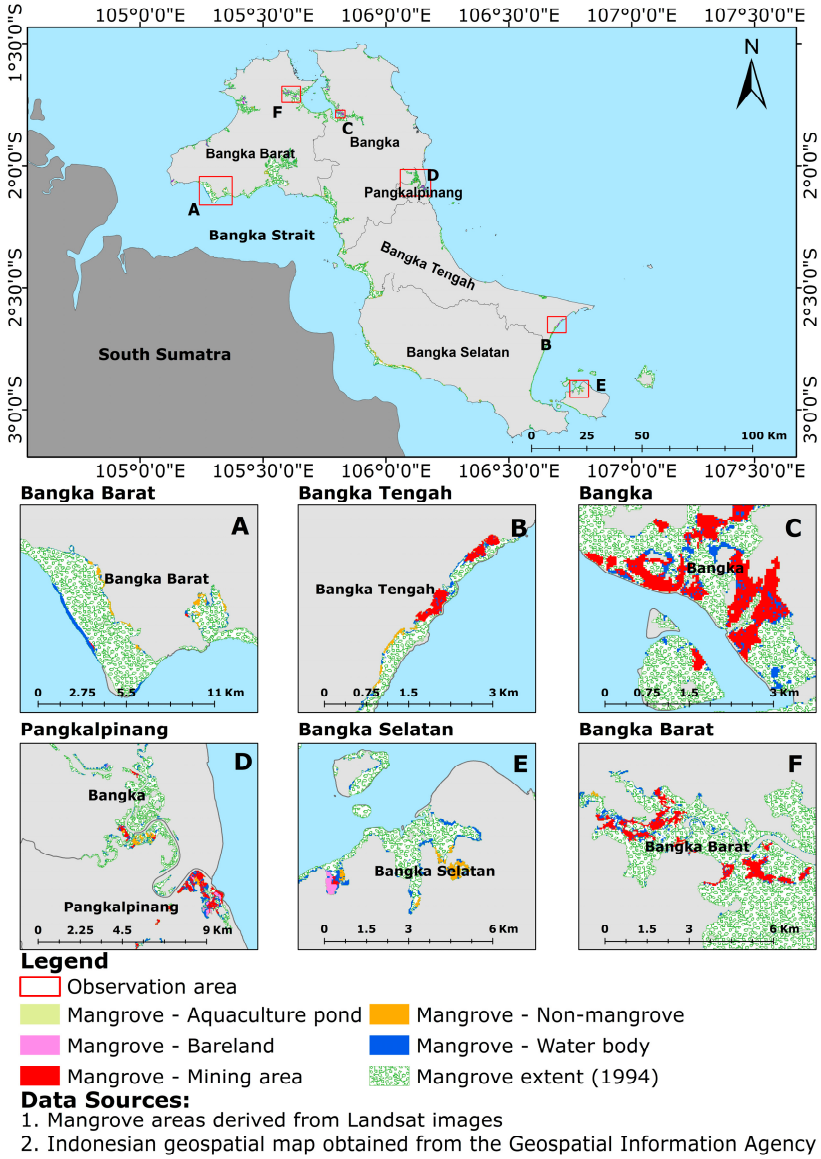

Figure 5. Mangrove area changes on Bangka Island between 1994 and 2023, highlighting key drivers of mangrove loss. Changes are shown island-wide for spatial context, while panels (**A**–**F**) present detailed patterns within the selected observation areas. The observation areas represent major regions, including Bangka Barat (**A**,**F**), Bangka Tengah (**B**), Bangka (**C**,**E**), and Pangkalpinang (**D**).

3.4.2. Map-to-Image

The change detection analysis based on NDVI anomaly revealed variations in mangrove extent over 30-year period (Figure 6). By comparing the NDVI values from different time intervals with the long-term average, areas with both positive and negative anomalies were identified. Areas with positive NDVI anomalies, where current values exceeded

the long-term average, indicated zones of mangrove growth or recovery. For example, in Bangka Barat and Bangka Tengah regencies (Figure 6A,B), these positive anomalies corresponded to mangrove expansion, primarily towards the sea. Conversely, negative NDVI anomalies, where current values fell below the long-term average, highlighted regions experiencing mangrove loss or degradation. In areas such as Bangka and Bangka Barat regencies (Figure 6C,F), this loss was associated with factors such as tin mining operations. These NDVI anomaly results complement the map-to-map change detection by providing additional information on vegetation condition changes that may not immediately appear as a complete class transition in mangrove extent maps.

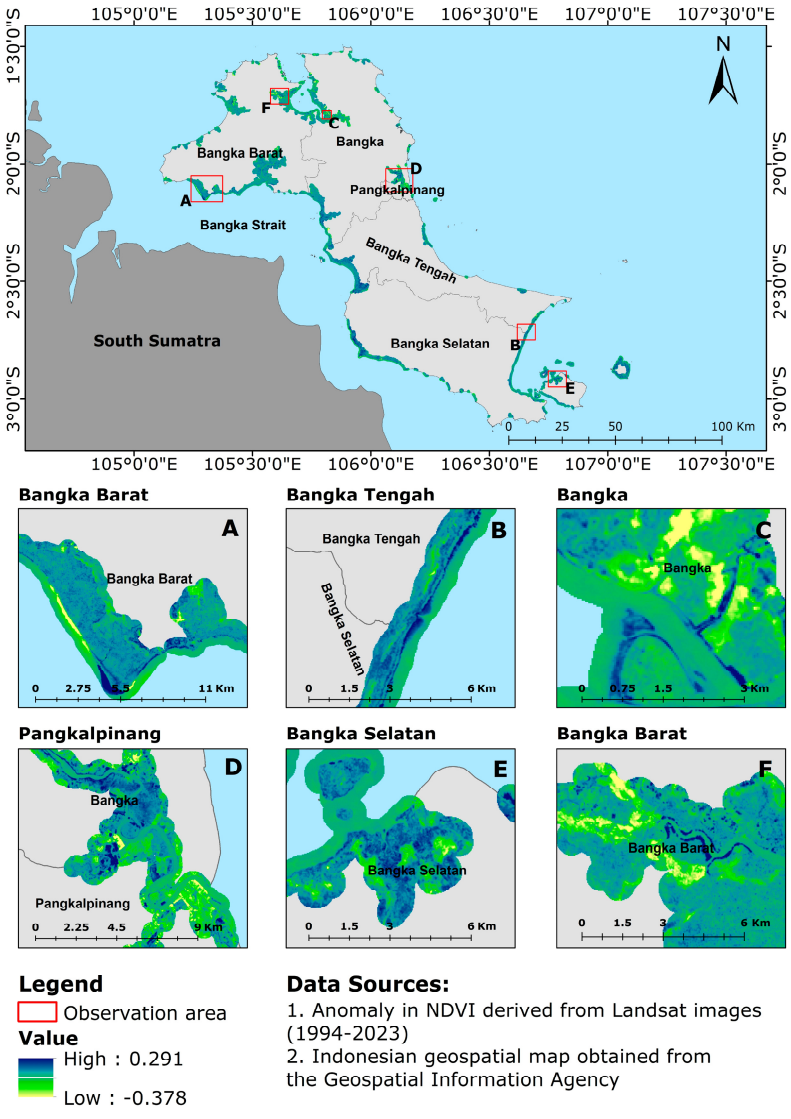

Figure 6. NDVI anomaly–based change detection on Bangka Island over the 30-year period (1994–2023). NDVI anomalies are shown island-wide for spatial context, while panels (**A**–**F**) present detailed anomaly patterns within the selected observation areas indicated in the main map.

3.5. LandTrendr Analysis for Detecting Disturbance and Recovery Periods

The LandTrendr analysis identified the periods of mangrove change due to disturbance and recovery on Bangka Island. For example, mangrove expansion in Bangka Barat and Bangka Tengah regencies occurred between 1989 and 1993 and has continued since then, as evidenced by map-to-map and NDVI anomaly change detection (Figures 6A,B and 7A,B). Conversely, mangrove loss in Bangka regency, attributed to tin mining activities, has been ongoing since 1996 (Figure 7C,F). Since LandTrendr detects

disturbance and recovery trajectories at the pixel level, disturbance and recovery events may occur simultaneously in different locations across the study area. However, LandTrendr was unable to detect the disturbance period related to erosion along the shoreline of Bangka Barat regency. This is likely because the erosion process is associated with shoreline retreat and sediment dynamics rather than abrupt changes in vegetation canopy, resulting in a weak NDVI signal that cannot be clearly segmented by the LandTrendr algorithm.

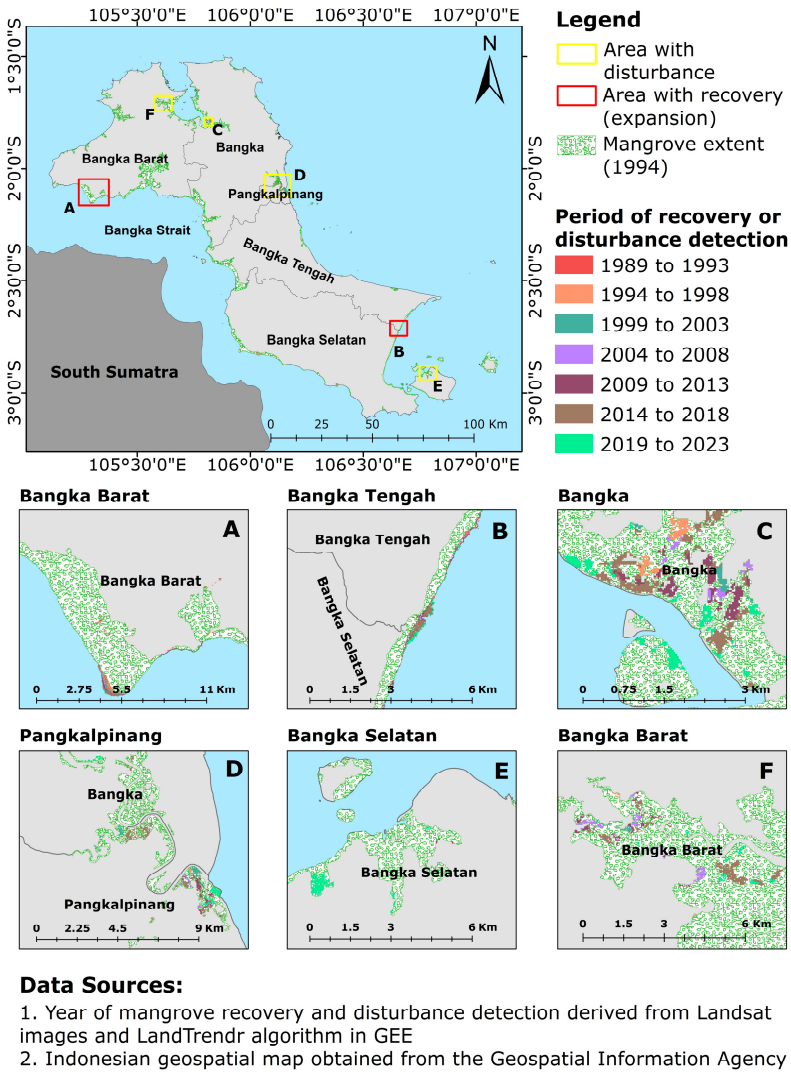

Figure 7. Detection periods of mangrove recovery and disturbance on Bangka Island over the 30-year study period (1994–2023). Areas of disturbance (yellow boxes) and recovery (red boxes) are indicated on the island-wide map for spatial context, while panels (**A**–**F**) present detailed patterns within selected observation areas: (**A**) Bangka Barat; (**B**) Bangka Tengah; (**C**) Bangka; (**D**) Pangkalpinang; (**E**) Bangka Selatan; and (**F**) Bangka Barat.

4. Discussion

This study conducted Landsat-based diachronic mapping of mangroves on Bangka Island over a 30-year period (1994–2023). The objective was to establish a 1994 baseline mangrove area map and analyze historical changes by comparing global datasets with the annual maps developed in this study. Changes in mangrove area were assessed using both map-to-map and map-to-image change detection approaches. Map-to-map change detection identified regions of mangrove gain and loss, which were further examined to determine spatial patterns and potential drivers. Results of the map-to-map analysis guided the delineation of areas of interest (AOIs) for NDVI anomaly-based map-to-image

assessment, where negative anomalies indicated loss and positive anomalies reflected growth or recovery.

LandTrendr analysis was employed to determine the timing of mangrove area changes, although it was less effective in identifying specific drivers. Nevertheless, the analysis revealed consistent periods of mangrove expansion beginning in 1989 and continuing throughout the study period. Overall, the findings provide a comprehensive assessment of mangrove area dynamics on Bangka Island, shaped by both natural processes and anthropogenic influences.

4.1. Accuracy Assessment of the Mangrove Extent Map for Bangka Island

The high accuracy of the annual mangrove maps can be attributed to precise AOI delineation, elevation masking, and a knowledge-based approach to collecting training samples prior to classification. Accurate AOI delineation focuses the analysis on areas where mangroves are likely to occur, reducing the inclusion of irrelevant land cover types. Although threshold-based maps have limitations in terms of misclassification, they remain valuable for identifying potential mangrove areas. These resources support the sampling process by facilitating mangrove detection, simplifying the generation of training samples, and defining AOI for further analyses.

The accuracy assessment results indicate consistently high classification performance throughout the study period, with overall accuracy ranging from 94% to 98.7%. Producer accuracy for the mangrove class remained particularly high, generally above 97%, indicating that most reference mangrove pixels were correctly identified by the classifier. This suggests that omission errors for mangrove areas were minimal across the 30-year time series.

Elevation masking excludes areas at unsuitable elevations, as mangroves typically occur in low-lying coastal zones subject to tidal inundation. Additionally, indices such as LSWI and MNDWI filter out water features [66,67], while NDVI and EVI distinguish vegetation from non-vegetated land covers [68]. These preprocessing steps refine the dataset, focusing the analysis on vegetation within appropriate coastal zones. By applying these filters prior to classification, misclassifications are minimized, and the workflow is streamlined to detect actual mangrove pixels, improving overall accuracy.

Despite the high accuracy obtained in this study, some uncertainty may remain in heterogeneous coastal environments where mangroves occur alongside other vegetation types or transitional land covers. Spectral similarities between mangroves and surrounding vegetation, such as shrubs, aquaculture ponds with vegetation, or sparsely vegetated tidal flats, can introduce minor classification ambiguities in optical satellite imagery. However, these cases represent a relatively small proportion of the mapped area and did not substantially affect the overall classification performance.

In this context, the Random Forest (RF) classifier has been widely used for mangrove mapping because of its ability to distinguish complex spectral patterns across multiple predictors. Previous studies have demonstrated its effectiveness in identifying and classifying mangrove forests using various satellite imagery and data inputs. For instance, integrating seasonal optical and synthetic aperture radar (SAR) data from Sentinel-1 and Sentinel-2 satellites for mapping mangrove ecosystems in the Hara protected area, Qeshm, Iran, achieved an overall accuracy of approximately 93.3% [69]. Furthermore, combining RF with other methods or indices, such as the MVI, MMRI, elevation data, and knowledge-based approaches, has been shown to improve the detection of mangrove changes, highlighting the benefits of integrating RF classification with additional spectral indices and auxiliary data [32,33,58,70–72].

4.2. Baseline Map and Spatial Distribution of Mangrove Forests on Bangka Island

The baseline map shows that mangrove coverage is primarily concentrated in the northern and western parts of Bangka Island. These regions include several areas officially designated as conserved and protected forests (Figure A1). The 2023 land cover map further indicates that areas adjacent to and within mangrove habitats are impacted by tin mining activities. Tin mining, a long-standing and economically important industry on Bangka Island, has likely altered mangrove extent over time. Because historical documentation on these impacts is limited, satellite-based observations provide important evidence for reconstructing land-use history and assessing the long-term effects of mining on mangrove ecosystems.

4.3. Comparison of Annual Maps from Various Global Datasets

Notable discrepancies were observed between the annual mangrove maps produced in this study and existing global datasets (Table 1 and Figure 3). These differences likely reflect variations in satellite data sources, spatial resolution, mapping approaches, and the temporal coverage of the datasets. Global products are typically designed for large-scale applications, which may limit their ability to capture smaller or fragmented mangrove patches in complex coastal environments. At the same time, very small or sparsely vegetated mangrove stands may remain difficult to detect even in locally derived maps using optical satellite imagery.

Because global mangrove datasets are widely used in research and decision-making, such inconsistencies can influence analytical outcomes and potentially affect management decisions. For example, discrepancies in mapped mangrove boundaries may influence the identification of priority areas for restoration or protection, particularly in small islands or fragmented coastal zones. In this context, locally derived mangrove maps can complement global datasets by providing additional spatial detail to support site-level planning and monitoring.

Accurate mangrove maps support the detection of area change, modelling of species distribution shifts, and the development of targeted conservation strategies [73,74]. Their practical importance is evident in applications worldwide: in Senegal, mapping has guided reforestation by clarifying zonation patterns, while in China, fine-scale assessments have revealed fragmented patches that shape local conservation planning [75,76]. These maps play a central role in monitoring and management, and their value increases when paired with local ecological knowledge.

4.4. Change Detection

The assessment of mangrove area changes over five-year intervals and a 30-year period (1994–2023) through map-to-map change detection reveals a complex pattern of mangrove dynamics. Although mangroves expanded by 4956.39 ha, representing a 10.30% gain relative to the baseline (1994), mangrove loss during the same period resulted in an overall net decline in mangrove extent (Table 1 and Figure 4).

Results reveal important temporal and spatial variability in mangrove area change. An exception to the general declining trend occurred during the 2004–2009 period, when mangrove gain slightly exceeded mangrove loss (Table 2). The spatial distribution of these gains indicates that they were mainly associated with seaward expansion in several coastal areas, including Bangka Barat and Bangka Tengah. Such expansion may reflect favorable local coastal conditions, including sediment deposition and natural mangrove colonization during that period.

For example, in the Bangka Barat (Tanjung Punai) and Bangka Tengah regencies, mangroves have expanded seaward by approximately 500 m and 200 m, respectively, over

the 30-year period (Figure 4A,B). This seaward expansion could be attributed to successful conservation efforts or other favorable ecological processes. Notably, Tanjung Punai, where significant expansion is observed, is one of the sampling sites included in the previous ecology study [47]. This site is dominated by *Sonneratia alba*, a species whose presence and expansion in seaward zones indicates regular saltwater inundation and ongoing silt deposition [77], a process possibly reduced or reversed by sea level rise.

In contrast, substantial mangrove loss has been observed in other areas, particularly in Bangka Barat regency, where erosion has resulted in a reduction in mangrove area by approximately 200 m (Figure 5A). Additionally, in Bangka regency, the expansion of tin mining activities from inland to offshore has strongly decreased mangrove area (Figure 5C), highlighting the detrimental effects of human activities on mangrove ecosystems. Additionally, tin mining operations are typically conducted near water bodies because the extraction process involves washing tin sand, which requires a water source (Figure A5). This process releases effluent into nearby rivers and coastal waters, leading to increased sedimentation and water contamination. Persistent tin mining may further alter hydrological conditions, leading to increased saltwater intrusion, altered mangrove composition, and potential landward shift (Figure A6). It should also be noted that mangrove decline may involve not only areal loss but also changes in species composition or ecological condition, which are not captured by the mapping approach used in this study.

Changes in mangrove area, whether expansion seaward or landward, are also seen in other regions globally. For example, seaward expansion has been reported in the Gulf of Carpentaria, Australia [78], Porong River, East Java [79], the coastline of Demak, Central Java [80], Parita Bay, Panama [81], and the Nanliu River estuary, China [82]. Conversely, landward expansion has been observed in the conterminous United States (CONUS) over approximately 35 years [83], in Amazon coastal wetlands [84], and along the Texas Gulf Coast [85].

Mangrove gain and loss are influenced by a range of factors, depending on local conditions. In East Africa, for instance, mangroves have demonstrated potential for landward shift under moderate sea level rise scenarios, though extreme rises could lead to significant loss, specifically in areas of future coastal squeeze [86]. Similarly, in the Amazon, mangroves have expanded into higher tidal flats in response to rising sea levels, but this expansion is limited by topographical constraints [87]. In South Africa, substrate elevation changes and sea storm events have been shown to influence mangrove distribution, with potential habitat loss occurring if sediment accretion is insufficient [88]. While increased inundation may enhance sedimentation rates and help some mangrove areas maintain their elevation relative to rising sea levels, insufficient sediment supply can result in mangrove drowning and erosion [89,90].

Climate change significantly impacts mangrove distribution by altering the hydrological cycle, which increases saltwater intrusion into previously freshwater areas, thereby promoting mangrove growth [84]. Increased tidal inundation can also facilitate landward expansion by reducing porewater salinity, which is beneficial for mangroves [87]. Additionally, milder winters and rising sea levels support the poleward shift of mangroves at range limits [83,91]. Other contributing factors include sediment accumulation, mangrove planting efforts, and changes in rainfall patterns, which can drive both seaward and landward expansion [78,81]. Conversely, severe erosion due to sea level rise has led to significant mangrove loss in some regions, with human activities being a factor in recent times [92]. For example, long-term shoreline analysis at Mui Ca Mau, Vietnam, revealed sustained erosion rates exceeding 30 m yr^{-1} along the exposed East Sea coast, resulting in extensive mangrove retreat, while simultaneous accretion on the sheltered Gulf of Thailand coast promoted mangrove expansion [93].

4.5. Study Implications

This study supports effective mangrove management by mapping patterns of loss and gain and identifying potential drivers. The resulting mangrove change database (https://sucipuspita1332.users.earthengine.app/view/mangrovebangka (accessed on 30 January 2026) for Mangrove Bangka Map 1 and https://sucipuspita1332.users.earthengine.app/view/mangrovebangka2 (accessed on 30 January 2026) for Mangrove Bangka Map 2) provides a foundation for assessing the impacts of human and natural influences, tracking distribution shifts, and predicting future trends [83,87]. Differences between mangrove maps produced in this study and existing global datasets also have practical implications for coastal management. In several locations, particularly small islands and fragmented coastal zones, the global datasets did not capture some mangrove areas that were identified in the annual maps developed here. Such differences may influence how restoration or protection priorities are determined, especially when mangrove distribution is used to guide site selection for rehabilitation programs. Locally derived maps can therefore provide additional spatial detail that helps managers better identify areas that require conservation or restoration.

On Bangka Island, many rehabilitation and restoration projects have been implemented without adequate site assessments and relied heavily on monospecific planting. Integrating insights from this database with detailed field evaluations can support more suitable site selection, guide species choices, and promote ecologically sound restoration strategies. Continued mapping and monitoring will be necessary to refine these approaches and strengthen long-term mangrove management.

4.6. Study Limitation

While this study achieved high accuracy in detecting mangrove extent, it did not capture some small mangrove patches (Figure A7), including those at Pangkul Beach reported in the previous study [47]. These areas are also absent from the global datasets used here, likely due to misclassification of sparse vegetation and interference from invasive species, which reduce spectral separability even when using advanced mangrove indices. As a result, small or low-density stands may be underrepresented in both our maps and global datasets.

This limitation underscores that, although remote sensing is invaluable for large-scale mapping and monitoring, it may overlook smaller or less dense mangrove patches. Integrating remote sensing with field-based assessments (e.g., ground-truthing and ecological field surveys) is therefore necessary to achieve a more comprehensive understanding of mangrove distribution and condition on Bangka Island.

5. Conclusions

This study provides a comprehensive assessment of mangrove dynamics on Bangka Island over a 30-year period by integrating Landsat-based mapping, change detection, and comparative analysis with global datasets. The results highlight substantial spatial and temporal variability, shaped by both natural processes and human activities such as tin mining and coastal erosion. While many areas experienced seaward expansion, others showed pronounced loss, underscoring the need for locally informed management. The high accuracy of the annual maps and the resulting mangrove-change database offer valuable resources for assessing pressures, planning restoration, and supporting long-term monitoring. However, limitations remain in detecting small or low-density stands, emphasizing the importance of combining remote sensing with detailed field assessments. Indeed, where gains and losses take place, resp. floristic composition and ecological quality may be very different and areal decline alone will not reflect the full impacts of observed dynam-

ics. These findings strengthen the evidence base for sustainable mangrove management and provide a solid foundation for future ecological and conservation-oriented studies on Bangka Island.

Author Contributions: Conceptualization, S.P.S., N.K., T.V.d.S. and F.V.C.; methodology, S.P.S., N.K., T.V.d.S. and F.V.C.; formal analysis, S.P.S.; investigation, S.P.S.; resources, S.P.S.; data curation, S.P.S.; writing—original draft preparation, S.P.S.; writing—review and editing, S.P.S., N.K., T.V.d.S. and F.V.C.; visualization, S.P.S.; supervision, N.K., T.V.d.S. and F.V.C. All authors have read and agreed to the published version of the manuscript.

Funding: This research was funded by the operational research fund from the Ministry of Education, Culture, Research, and Technology of the Republic of Indonesia, through Beasiswa Program Pascasarjana Luar Negeri (BPPLN), Contract No. T/985/D3.2/KD.02.01/2019 (9 September 2019).

Data Availability Statement: Landsat imagery is publicly available through the Google Earth Engine data catalogue. Global mangrove datasets used for comparison are publicly accessible online through their respective sources. The Google Earth Engine Apps developed for this study can be accessed at https://sucipuspita1332.users.earthengine.app/view/mangrovebangka, accessed on 30 January 2026 (Mangrove Bangka Map 1) and https://sucipuspita1332.users.earthengine.app/view/mangrovebangka2, accessed on 30 January 2026 (Mangrove Bangka Map 2). The Google Earth Engine implementation developed for this study relies on project-specific assets (e.g., training samples and ancillary layers) that cannot be fully redistributed. Therefore, the code and derived mangrove extent and change maps are available from the corresponding author upon reasonable request.

Acknowledgments: The authors thank Gladys Villegas and Jasper Feyen for their valuable feedback and insights based on their experience with mapping using the Google Earth Engine platform.

Conflicts of Interest: The authors declare no conflicts of interest. The funders had no role in the design of the study; in the collection, analyses, or interpretation of data; in the writing of the manuscript; or in the decision to publish the results.

Appendix A

Table A1. Landsat 5 TM, 7 ETM+, and 8 OLI/TIRS spectral bands.

Band	Landsat 5 TM		Landsat 7 ETM+		Landsat 8 OLI/TIRS	
	Wavelength (μm)	**Resolution (m)**	**Wavelength (μm)**	**Resolution (m)**	**Wavelength (μm)**	**Resolution (m)**
Band 1	0.45–0.52 (Blue)	30	0.45–0.52 (Blue)	30	0.43–0.45 (Coastal)	30
Band 2	0.52–0.60 (Green)	30	0.52–0.60 (Green)	30	0.45–0.51 (Blue)	30
Band 3	0.63–0.69 (Red)	30	0.63–0.69 (Red)	30	0.53–0.59 (Green)	30
Band 4	0.76–0.90 (NIR)	30	0.77–0.90 (NIR)	30	0.64–0.67 (Red)	30
Band 5	1.55–1.75 (SWIR 1)	30	1.55–1.75 (SWIR 1)	30	0.85–0.88 (NIR)	30
Band 6	10.40–12.50 (Thermal)	120 (resampled to 30)	10.40–12.50 (Thermal)	60 (resampled to 30)	1.57–1.65 (SWIR 1)	30
Band 7	2.08–2.35 (SWIR 2)	30	2.09–2.35 (SWIR 2)	30	2.11–2.29 (SWIR 2)	30
Band 8			0.52–0.90	15	0.50–0.68 (Panchromatic)	15
Band 9					1.36–1.38 (Cirrus)	30
Band 10					10.6–11.19 (TIRS 1)	100 (resampled to 30)
Band 11					11.50–12.51 (TIRS 2)	100 (resampled to 30)

Note: NIR (Near Infrared); SWIR (Shortwave Infrared); OLI (Operational Land Imager); TIRS (Thermal Infrared); source: https://www.usgs.gov/faqs/what-are-band-designations-landsat-satellites (accessed on 13 June 2024).

Table A2. Summary of the satellite images used in this study.

Sensor	Start Year	Study Period (Year)	Total Number of Images
Landsat 5 TM	1994	1	123
	1995	1	144
	1996	1	142
	1997	1	159
	1998	1	168
	1999	1	151
	2000	2	224
	2001	2	191
	2005	1	146
	2006	1	162
	2007	1	149
	2008	1	119
	2009	1	135
	2010	2	156
Landsat 7 ETM+	2002	1	162
	2003	2	202
	2004	2	196
	2011	4	184
	2012	4	215
	2013	4	235
Landsat 8 OLI	2014	1	168
	2015	–	103
	2016	1	205
	2017	–	95
	2018	1	188
	2019	1	197
	2020	1	185
	2021	1	164
	2022	1	162
	2023	2	253

Table A3. Spectral indices applied to the annual cloud-free composite images.

Index	Formula	Reference
Mangrove		
Automatic Mangrove Map and Index	$AMMI = \frac{\text{NIR}-\text{Red}}{\text{Red}+\text{SWIR1}} \times \frac{\text{NIR}-\text{SWIR1}}{\text{SWIR1}-0.65\times\text{Red}}$	Suyarso (2022) [94]
Mangrove Index	$\text{MI} = \frac{\text{NIR}-\text{SWIR}}{\text{NIR}\times\text{SWIR}} \times 10,000$	Winarso and Purwanto (2014) [95]
Modular Mangrove Recognition Index	$\text{MMRI} = \frac{\text{MNDWI}-\text{NDVI}}{\text{NDWI}+\text{NDVI}}$	Diniz et al. (2019) [70]
Mangrove Vegetation Index	$\text{MVI} = \frac{\text{NIR}-\text{Green}}{\text{SWIR1}-\text{Green}}$	Baloloy et al. (2020) [71]
Vegetation and water		
Normalized Difference Vegetation Index	$\text{NDVI} = \frac{\text{NIR}-\text{Red}}{\text{NIR}+\text{Red}}$	Rouse et al. (1974) [96]
Normalized Difference Water Index	$\text{NDWI} = \frac{\text{Green}-\text{NIR}}{\text{Green}+\text{NIR}}$	McFeeters (1996) [97]
Modified Normalized Difference Water Index	$\text{MNDWI} = \frac{\text{Green}-\text{SWIR1}}{\text{Green}+\text{SWIR1}}$	Xu (2006) [66]
Enhanced Vegetation Index	$\text{EVI} = 2.5 \times \frac{\text{NIR}-\text{Red}}{\text{NIR}+6\times\text{Red}-7.5\times\text{Blue}+1}$	Huete et al. (1997) [68]
Land Surface Water Index	$\text{LSWI} = \frac{\text{NIR}-\text{SWIR}}{\text{NIR}+\text{SWIR}}$	Gao (1996) [98]; Xiao et al. (2004) [99]
Green Chlorophyll Vegetation Index	$\text{GCVI} = \left(\frac{\text{NIR}}{\text{Green}}\right) - 1$	Gitelson et al. (2005) [100]
Simple Ratio	$\text{SR} = \frac{\text{NIR}}{\text{Red}}$	Jordan (1969) [101]

Table A4. Bands used in spectral indices based on Landsat sensors.

Band	Landsat 5 TM and 7 ETM+		Landsat 8 OLI/TIRS	
	Band Number	Wavelength (μm)	Band Number	Wavelength (μm)
Green	Band 2	0.52–0.60	Band 3	0.53–0.59
Red	Band 3	0.63–0.69	Band 4	0.64–0.67
NIR	Band 4	0.76–0.90	Band 5	0.85–0.88
SWIR1	Band 5	1.55–1.75	Band 6	1.57–1.65

Table A5. Accuracy assessment results for annual mangrove extent mapping (1994–2023).

Year	Overall Accuracy (%)	Producer Accuracy (%)		User Accuracy (%)	
		Non-Mangrove	Mangrove	Non-Mangrove	Mangrove
1994	98.3	96.8	100.0	100.0	96.7
1995	97.0	94.3	100.0	100.0	94.0
1996	96.3	93.7	99.3	99.3	93.3
1997	95.3	91.5	100.0	100.0	90.7
1998	96.0	92.6	100.0	100.0	92.0
1999	95.0	90.9	100.0	100.0	90.0
2000	95.3	91.5	100.0	100.0	90.7
2001	95.7	92.0	100.0	100.0	91.3
2002	97.0	95.5	98.6	98.7	95.3
2003	96.7	94.3	99.3	99.3	94.0
2004	97.0	94.9	99.3	99.3	94.7
2005	96.7	94.3	99.3	99.3	94.0
2006	98.7	97.4	100.0	100.0	97.3
2007	94.0	94.6	93.4	93.3	94.7
2008	97.0	94.3	100.0	100.0	94.0
2009	97.7	96.7	98.6	98.7	96.7
2010	97.3	94.9	100.0	100.0	94.7
2011	97.3	95.5	99.3	99.3	95.3
2012	96.3	94.3	98.6	98.7	94.0
2013	96.7	94.3	99.3	99.3	94.0
2014	96.0	94.2	97.9	98.0	94.0
2015	95.7	94.2	97.2	97.3	94.0
2016	96.3	93.7	99.3	99.3	93.3
2017	96.7	93.8	100.0	100.0	93.3
2018	95.3	93.0	97.9	98.0	92.7
2019	95.0	91.4	99.3	99.3	90.7
2020	95.0	91.9	98.6	98.7	91.3
2021	97.0	94.9	99.3	99.3	94.7
2022	98.3	96.8	100.0	100.0	96.7
2023	96.0	94.2	97.9	98.0	94.0

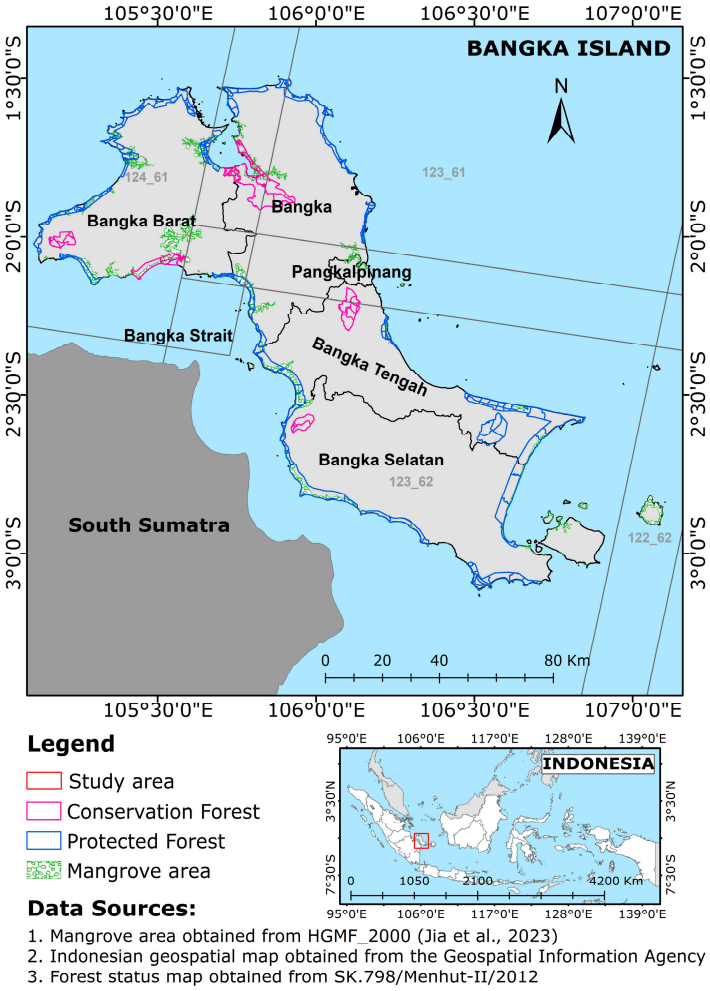

Figure A1. Study area, spatial distribution of mangroves from Jia et al. (2023) [38], and coverage of Landsat Worldwide Reference System-2 (WRS-2) path/row on Bangka Island.

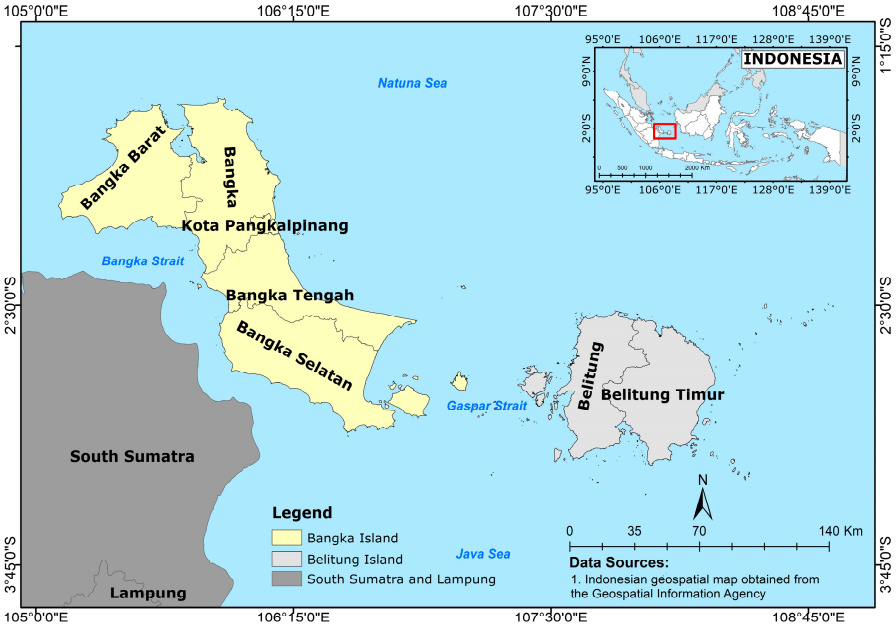

Figure A2. Map of Bangka Belitung Province, highlighting Bangka Island (yellow) bordered by the Gaspar Strait to the east, the Bangka Strait to the west, the Java Sea to the south, and the Natuna Sea to the north.

Figure A3. Comparison of false color composite images: initial (**left**) and after applying elevation masking and filtering criteria (**right**) to focus on mangrove regions.

Figure A4. Example of a Landsat false color composite image (1994) on GEE, showing mangrove (green) and non-mangrove (yellow) reference samples.

Figure A5. 'Unconventional tin mining' operations on Bangka Island: (**A**) Offshore platforms extracting tin sand from the seabed (Jebu Laut, 25 August 2021); (**B**) Onshore tin washing process, where tin sand is washed to separate tin from other materials (Bangka Tengah Regency, 9 August 2022); Photos by Suci Puspita Sari.

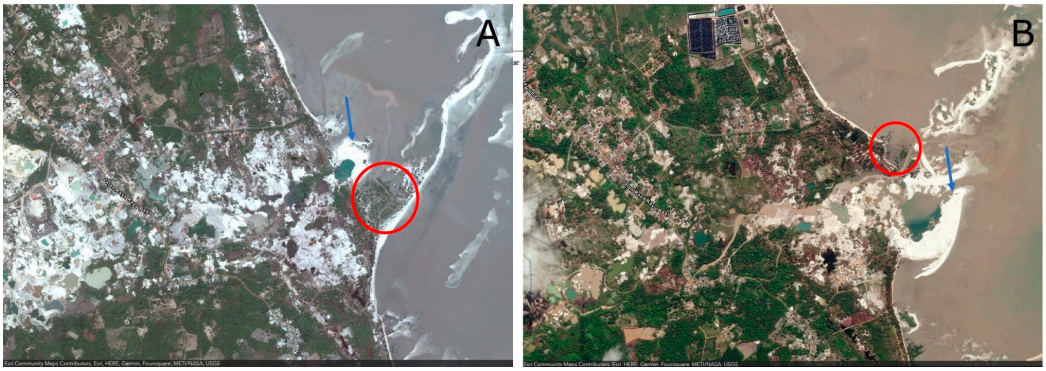

Figure A6. Comparative visual understanding of tin mining activities (mines and mine tailing) impact on mangrove spatial distribution changes at Pangkul Beach. The red circle highlights change in the coastal area, and the blue arrow points to tin mining tailings: (**A**) September 2011; (**B**) July 2019. Note that the tidal phase may be different in both images and not all differences correspond to differences in the field. Background imagery: Esri Community Maps Contributors, Esri, HERE, Garmin, Foursquare, METI/NASA, USGS.

Figure A7. Small and sparse mangrove patches at Pangkul Beach, viewed from the terrestrial side in August 2022, with terrestrial *Casuarina equisetifolia* present in the landscape; Photo by Suci Puspita Sari.

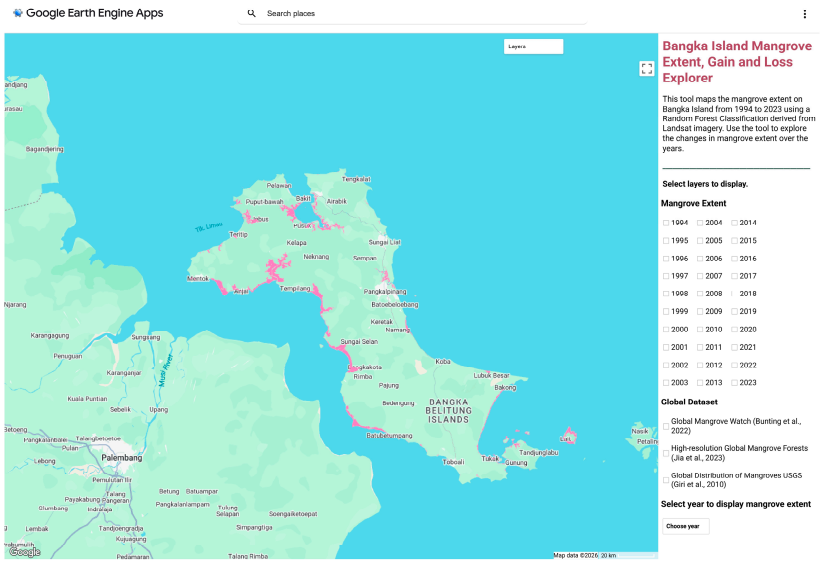

Figure A8. Google Earth Engine (GEE) App interface for visualizing annual mangrove extent maps on Bangka Island (1994–2023) and comparing results with selected global mangrove datasets [10,38,54]. The application is available at: https://sucipuspita1332.users.earthengine.app/view/mangrovebangka2 (accessed on 30 January 2026).

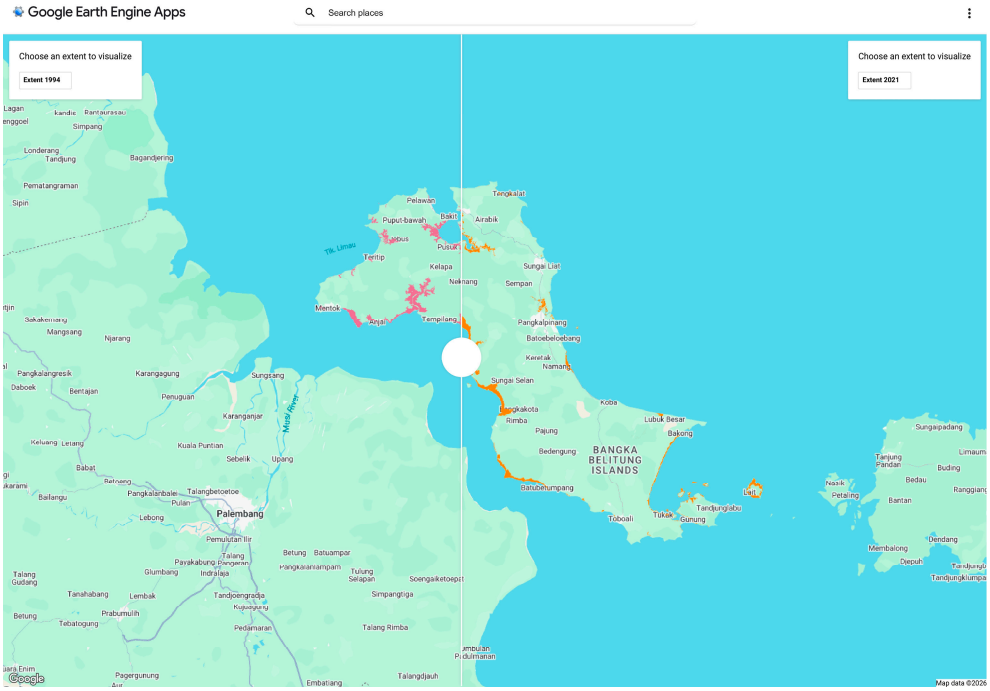

Figure A9. Google Earth Engine (GEE) App interface with a swipe/slider tool for comparing mangrove extent maps on Bangka Island between two selected years (1994–2023). The application is available at: https://sucipuspita1332.users.earthengine.app/view/mangrovebangka (accessed on 30 January 2026).

References

1. Polidoro, B.A.; Carpenter, K.E.; Collins, L.; Duke, N.C.; Ellison, A.M.; Ellison, J.C.; Farnsworth, E.J.; Fernando, E.S.; Kathiresan, K.; Koedam, N.E.; et al. The Loss of Species: Mangrove Extinction Risk and Geographic Areas of Global Concern. *PLoS ONE* **2010**, *5*, e10095. [CrossRef]
2. Giri, C. Recent Advancement in Mangrove Forests Mapping and Monitoring of the World Using Earth Observation Satellite Data. *Remote Sens.* **2021**, *13*, 563. [CrossRef]
3. Tomlinson, P.B. *The Botany of Mangroves*, 2nd ed.; Cambridge University Press: Cambridge, UK, 2016; ISBN 9781139946575.
4. Spalding, M.; Kainuma, M.; Collins, L. *World Atlas of Mangroves*; Routledge: London, UK, 2010. [CrossRef]
5. Donato, D.C.; Boone Kauffman, J.; Murdiyarso, D.; Kurnianto, S.; Kanninen, M. Mangroves among the Most Carbon-Rich Forests in the Tropics. *Nat. Geosci.* **2011**, *4*, 293–297. [CrossRef]
6. Pendleton, L.; Donato, D.C.; Murray, B.C.; Crooks, S.; Jenkins, W.A.; Sifleet, S.; Craft, C.; Fourqurean, J.W.; Kauffman, J.B.; Marbà, N.; et al. Estimating Global "Blue Carbon" Emissions from Conversion and Degradation of Vegetated Coastal Ecosystems. *PLoS ONE* **2012**, *7*, e43542. [CrossRef]
7. Alongi, D.M. Global Significance of Mangrove Blue Carbon in Climate Change Mitigation. *Sci* **2020**, *2*, 67. [CrossRef]
8. Bryan-Brown, D.N.; Connolly, R.M.; Richards, D.R.; Adame, F.; Friess, D.A.; Brown, C.J. Global Trends in Mangrove Forest Fragmentation. *Sci. Rep.* **2020**, *10*, 7117. [CrossRef] [PubMed]
9. Das, S.C.; Das, S.; Tah, J. Mangrove Ecosystems and Their Services. In *Mangroves: Biodiversity, Livelihoods and Conservation*; Springer Nature: Singapore, 2022; pp. 139–152. ISBN 9789811905186. [CrossRef]
10. Bunting, P.; Rosenqvist, A.; Hilarides, L.; Lucas, R.M.; Thomas, N.; Tadono, T.; Worthington, T.A.; Spalding, M.; Murray, N.J.; Rebelo, L.-M. Global Mangrove Extent Change 1996–2020: Global Mangrove Watch Version 3.0. *Remote Sens.* **2022**, *14*, 3657. [CrossRef]
11. Goldberg, L.; Lagomasino, D.; Thomas, N.; Fatoyinbo, T. Global Declines in Human-Driven Mangrove Loss. *Glob. Change Biol.* **2020**, *26*, 5844–5855. [CrossRef]
12. Hamilton, S.E.; Casey, D. Creation of a High Spatio-Temporal Resolution Global Database of Continuous Mangrove Forest Cover for the 21st Century (CGMFC-21). *Glob. Ecol. Biogeogr.* **2016**, *25*, 729–738. [CrossRef]
13. Friess, D.A.; Rogers, K.; Lovelock, C.E.; Krauss, K.W.; Hamilton, S.E.; Lee, S.Y.; Lucas, R.; Primavera, J.; Rajkaran, A.; Shi, S. The State of the World's Mangrove Forests: Past, Present, and Future. *Annu. Rev. Environ. Resour.* **2019**, *44*, 89–115. [CrossRef]
14. Sidik, F.; Supriyanto, B.; Krisnawati, H.; Muttaqin, M.Z. Mangrove Conservation for Climate Change Mitigation in Indonesia. *Wiley Interdiscip. Rev. Clim. Change* **2018**, *9*, e529. [CrossRef]

15. Nordhaus, I.; Toben, M.; Fauziyah, A. Impact of Deforestation on Mangrove Tree Diversity, Biomass and Community Dynamics in the Segara Anakan Lagoon, Java, Indonesia: A Ten-Year Perspective. *Estuar. Coast. Shelf Sci.* **2019**, *227*, 106300. [CrossRef]
16. Direktorat Konservasi Tanah dan Air. *Peta Mangrove Nasional 2021*; Ministry of Environment and Forestry Republic Indonesia: Jakarta, Indonesia, 2021.
17. Arifanti, V.B.; Kauffman, J.B.; Subarno; Ilman, M.; Tosiani, A.; Novita, N. Contributions of Mangrove Conservation and Restoration to Climate Change Mitigation in Indonesia. *Glob. Change Biol.* **2022**, *28*, 4523–4538. [CrossRef]
18. Sari, S.P.; Rosalina, D. Mapping and Monitoring of Mangrove Density Changes on Tin Mining Area. *Procedia Environ. Sci.* **2016**, *33*, 436–442. [CrossRef]
19. Rosalina, D.; Rombe, K.H. Struktur Dan Komposisi Jenis Mangrove Di Kabupaten Bangka Barat. *J. Airaha* **2021**, *10*, 099–108. [CrossRef]
20. Farhaby, A.M.; Anwar, M.S. Analisis Kondisi Kesehatan Ekosistem Mangrove Di Pantai Takari Kabupaten Bangka. *Bioma Berk. Ilm. Biol.* **2022**, *24*, 147–154. [CrossRef]
21. Sari, S.P.; Feyen, J.; Koedam, N.; Van Coillie, F. Monitoring Trends of Mangrove Disturbance at the Tin Mining Area of Bangka Island Using Landsat Time Series and Landtrendr. In Proceedings of the IGARSS 2022—2022 IEEE International Geoscience and Remote Sensing Symposium, Kuala Lumpur, Malaysia, 17–22 July 2022; pp. 457–460.
22. Maulana Gerakkan Ekonomi Masyarakat Pesisir, KLHK Tanam Mangrove [Mobilising Coastal Community Economy, KLHK Plants Mangroves]. Available online: https://mediaindonesia.com/nusantara/348072/gerakkan-ekonomi-masyarakat-pesisir-klhk-tanam-mangrove (accessed on 26 January 2026).
23. Syahid, L.N.; Sakti, A.D.; Virtriana, R.; Wikantika, K.; Windupranata, W.; Tsuyuki, S.; Caraka, R.E.; Pribadi, R. Determining Optimal Location for Mangrove Planting Using Remote Sensing and Climate Model Projection in Southeast Asia. *Remote Sens.* **2020**, *12*, 3734. [CrossRef]
24. Murillo-Sandoval, P.J.; Fatoyinbo, L.; Simard, M. Mangroves Cover Change Trajectories 1984–2020: The Gradual Decrease of Mangroves in Colombia. *Front. Mar. Sci.* **2022**, *9*. [CrossRef]
25. Jia, M.; Wang, Z.; Wang, C.; Mao, D.; Zhang, Y. A New Vegetation Index to Detect Periodically Submerged Mangrove Forest Using Single-Tide Sentinel-2 Imagery. *Remote Sens.* **2019**, *11*, 2043. [CrossRef]
26. Spalding, M.D.; Fox, H.E.; Allen, G.R.; Davidson, N.; Ferdaña, Z.A.; Finlayson, M.; Halpern, B.S.; Jorge, M.A.; Lombana, A.; Lourie, S.A.; et al. Marine Ecoregions of the World: A Bioregionalization of Coastal and Shelf Areas. *BioScience* **2007**, *57*, 573–583. [CrossRef]
27. Troche-Souza, C.H.; Velázquez-Salazar, S.; Cruz-López, M.I.; Rodríguez-Zúñiga, M.T.; Alcántara-Maya, J.A.; Vázquez-Balderas, B.; Valderrama-Landeros, L.; Villeda-Chávez, E.; Ressl, R. Comments on Acosta-Velázquez et al. Changes in Mangrove Coverage Classification Criteria Could Impact the Conservation of Mangroves in Mexico. *Land Use Policy*, 2023, 129, 106651. *Land Use Policy* **2023**, *134*, 106883. [CrossRef]
28. Lagomasino, D.; Fatoyinbo, T.; Lee, S.; Feliciano, E.; Trettin, C.; Shapiro, A.; Mangora, M.M. Measuring Mangrove Carbon Loss and Gain in Deltas. *Environ. Res. Lett.* **2019**, *14*, 025002. [CrossRef]
29. Omar, H.; Misman, M.A.; Linggok, V. Characterizing and Monitoring of Mangroves in Malaysia Using Landsat-Based Spatial-Spectral Variability. *IOP Conf. Ser. Earth Environ. Sci.* **2018**, *169*, 012037. [CrossRef]
30. Otero, V.; Van De Kerchove, R.; Satyanarayana, B.; Mohd-Lokman, H.; Lucas, R.; Dahdouh-Guebas, F. An Analysis of the Early Regeneration of Mangrove Forests Using Landsat Time Series in the Matang Mangrove Forest Reserve, Peninsular Malaysia. *Remote Sens.* **2019**, *11*, 774. [CrossRef]
31. Gopalakrishnan, L.; Satyanarayana, B.; Chen, D.; Wolswijk, G.; Amir, A.A.; Vandegehuchte, M.; Muslim, A.; Koedam, N.; Dahdouh-Guebas, F. Using Historical Archives and Landsat Imagery to Explore Changes in the Mangrove Cover of Peninsular Malaysia between 1853 and 2018. *Remote Sens.* **2021**, *13*, 3403. [CrossRef]
32. Purwanto, A.D.; Wikantika, K.; Deliar, A.; Darmawan, S. Decision Tree and Random Forest Classification Algorithms for Mangrove Forest Mapping in Sembilang National Park, Indonesia. *Remote Sens.* **2022**, *15*, 16. [CrossRef]
33. Jamaluddin, I.; Chen, Y.-N.; Ridha, S.M.; Mahyatar, P.; Ayudyanti, A.G. Two Decades Mangroves Loss Monitoring Using Random Forest and Landsat Data in East Luwu, Indonesia (2000–2020). *Geomatics* **2022**, *2*, 282–296. [CrossRef]
34. Purwanto, A.D.; Wikantika, K.; Darmawan, S.; Deliar, A. Predicting the Distribution of Mangrove Forests through Random Forest Algorithm by Combining Spectral Features and DEM Data. *IOP Conf. Ser. Earth Environ. Sci.* **2023**, *1276*, 012002. [CrossRef]
35. Rahmadi, R.; Koestoer, R.H.S. Comparison of the Mangrove Forest Mapping Algorithms in Kelabat Bay Using Random Forest and Support Vector Machines. *Int. J. Remote Sens. Earth Sci. (IJReSES)* **2023**, *20*, 106–112. Available online: https://ejournal.brin.go.id/ijreses/article/view/13752 (accessed on 30 January 2026).
36. Long, J.B.; Giri, C. Mapping the Philippines' Mangrove Forests Using Landsat Imagery. *Sensors* **2011**, *11*, 2972–2981. [CrossRef]
37. Bunting, P.; Rosenqvist, A.; Lucas, R.M.; Rebelo, L.-M.; Hilarides, L.; Thomas, N.; Hardy, A.; Itoh, T.; Shimada, M.; Finlayson, C.M. The Global Mangrove Watch—A New 2010 Global Baseline of Mangrove Extent. *Remote Sens.* **2018**, *10*, 1669. [CrossRef]

38. Jia, M.; Wang, Z.; Mao, D.; Ren, C.; Song, K.; Zhao, C.; Wang, C.; Xiao, X.; Wang, Y. Mapping Global Distribution of Mangrove Forests at 10-m Resolution. *Sci. Bull.* **2023**, *68*, 1306–1316. [CrossRef]
39. Gouvêa, L.P.; Serrão, E.A.; Cavanaugh, K.; Gurgel, C.F.D.; Horta, P.A.; Assis, J. Global Impacts of Projected Climate Changes on the Extent and Aboveground Biomass of Mangrove Forests. *Divers. Distrib.* **2022**, *28*, 2349–2360. [CrossRef]
40. Lee, C.K.F.; Nicholson, E.; Duncan, C.; Grantham, H.S.; Keith, D.A.; Tizard, R.; Murray, N.J. Assessing the Conservation Status of Mangroves in Rakhine, Myanmar. *Aquat. Conserv.* **2024**, *34*. [CrossRef]
41. Cavanaugh, K.C.; Osland, M.J.; Bardou, R.; Hinojosa-Arango, G.; López-Vivas, J.M.; Parker, J.D.; Rovai, A.S. Sensitivity of Mangrove Range Limits to Climate Variability. *Glob. Ecol. Biogeogr.* **2018**, *27*, 925–935. [CrossRef]
42. Umroh; Adi, W.; Sari, S.P. Detection of Mangrove Distribution in Pongok Island. *Procedia Environ. Sci.* **2016**, *33*, 253–257. [CrossRef]
43. Savira, N.; Hartoko, A.; Adi, W. Perubahan Luasan Mangrove Pesisir Timur Kabupaten Bangka Tengah Menggunakan Citra Satelit ASTER. *Akuatik J. Sumberd. Perair.* **2018**, *12*, 53–60. [CrossRef]
44. Farhaby, A.M.; Muftiadi, M.R.; Supratman, O.; Adi, W. Pemetaan Kawasan Hutan Mangrove Menggunakan Drone Di Kawasan Wisata Hutan Mangrove Sebagai Salah Satu Upaya Konservasi Kawasan Hutan Mangrove Di Desa Tukak Kabupaten Bangka Selatan. *Akuatik: J. Sumberd. Perair.* **2022**, *16*, 6–9. Available online: https://journal.ubb.ac.id/akuatik/article/view/3881 (accessed on 30 January 2026).
45. BPS. *Provinsi Kepulauan Bangka Belitung Dalam Angka 2022*; Yuwono, B.S., Ilmiana, H.T., Firmandika, R., Nasrun, A., Eds.; BPS Provinsi Kepulauan Bangka Belitung: Provinsi Kepulauan Bangka Belitung, Indonesia, 2022. Available online: https://babel.bps.go.id/id/publication/2022/02/25/79d93d4f97fd1850c20d5685/provinsi-kepulauan-bangka-belitung-dalam-angka-2022.html (accessed on 30 January 2026).
46. Pramudji. *Mangrove di Indonesia*; Suharsono, Ed.; COREMAP-CTI LIPI: Jakarta, Indonesia, 2017; ISBN 9786026504081.
47. Sari, S.P.; Koedam, N.; Pamungkas, A.; Muftiadi, M.R.; Van Coillie, F. Unveiling the Diversity of Bangka Island's Mangroves: A Baseline for Effective Conservation and Restoration. *Forests* **2023**, *14*, 1666. [CrossRef]
48. Kottek, M.; Grieser, J.; Beck, C.; Rudolf, B.; Rubel, F. World Map of the Köppen-Geiger Climate Classification Updated. *Meteorol. Z.* **2006**, *15*, 259–263. [CrossRef]
49. BMKG. *Pemutakhiran Zona Musim Indonesia Periode 1991–2020*; Badan Meteorologi Klimatologi Dan Geofisika: Jakarta, Indonesia, 2022. Available online: https://iklim.bmkg.go.id/bmkgadmin/storage/buletin/Buku_ZOM9120_versi_cetak.pdf (accessed on 30 January 2026).
50. Knapp, K.R.; Kruk, M.C.; Levinson, D.H.; Diamond, H.J.; Neumann, C.J. The International Best Track Archive for Climate Stewardship (IBTrACS): Unifying Tropical Cyclone Data. *Bull. Am. Meteorol. Soc.* **2010**, *91*, 363–376. [CrossRef]
51. Hülsen, S.; Dee, L.E.; Kropf, C.M.; Meiler, S.; Bresch, D.N. Mangroves and Their Services Are at Risk from Tropical Cyclones and Sea Level Rise under Climate Change. *Commun. Earth Environ.* **2025**, *6*, 262. [CrossRef]
52. Radjawane, I.M.; Saputro, B.S.C.; Egon, A. Model Hidrodinamika Pasang Surut di Perairan Kepulauan Bangka Belitung. *J. Tek. Sipil* **2018**, *25*, 121–128. [CrossRef]
53. Handoko, E.Y.; Yuwono; Ariani, R. Analisis Kenaikan Muka Air Laut Indonesia Tahun 1993–2018 Menggunakan Data Altimetri. *Geoid* **2020**, *15*, 58–64. [CrossRef]
54. Giri, C.; Ochieng, E.; Tieszen, L.L.; Zhu, Z.; Singh, A.; Loveland, T.; Masek, J.; Duke, N. Status and Distribution of Mangrove Forests of the World Using Earth Observation Satellite Data. *Glob. Ecol. Biogeogr.* **2010**, *20*, 154–159. [CrossRef]
55. Hermosilla, T.; Francini, S.; Nicolau, A.P.; Wulder, M.A.; White, J.C.; Coops, N.C.; Chirici, G. Clouds and Image Compositing. In *Cloud-Based Remote Sensing with Google Earth Engine: Fundamentals and Applications*; Cardille, J.A., Crowley, M.A., Saah, D., Clinton, N.E., Eds.; Springer International Publishing: Cham, Switzerland, 2024; pp. 279–302, ISBN 9783031265884. [CrossRef]
56. Mondal, P.; Trzaska, S.; De Sherbinin, A. Landsat-Derived Estimates of Mangrove Extents in the Sierra Leone Coastal Landscape Complex during 1990–2016. *Sensors* **2017**, *18*, 12. [CrossRef]
57. Fatoyinbo, T.E.; Simard, M. Height and Biomass of Mangroves in Africa from ICESat/GLAS and SRTM. *Int. J. Remote Sens.* **2013**, *34*, 668–681. [CrossRef]
58. Chen, B.; Xiao, X.; Li, X.; Pan, L.; Doughty, R.; Ma, J.; Dong, J.; Qin, Y.; Zhao, B.; Wu, Z.; et al. A Mangrove Forest Map of China in 2015: Analysis of Time Series Landsat 7/8 and Sentinel-1A Imagery in Google Earth Engine Cloud Computing Platform. *ISPRS J. Photogramm. Remote Sens.* **2017**, *131*, 104–120. [CrossRef]
59. Purwanto, A.D.; Asriningrum, W. Identification of Mangrove Forests Using Multispectral Satellite Imageries. *Int. J. Remote Sens. Earth Sci. (IJReSES)* **2019**, *16*, 63–86. Available online: https://ejournal.brin.go.id/ijreses/article/view/13844 (accessed on 30 January 2026). [CrossRef]
60. Barenblitt, A.; Fatoyinbo, T. Remote Sensing for Mangroves in Support of the UN Sustainable Development Goals. NASA Applied Remote Sensing Training Program (ARSET), 2020. Available online: https://www.earthdata.nasa.gov/learn/trainings/remote-sensing-mangroves-support-un-sustainable-development-goals (accessed on 10 May 2021).

61. Thomas, N.; Bunting, P.; Lucas, R.; Hardy, A.; Rosenqvist, A.; Fatoyinbo, T. Mapping Mangrove Extent and Change: A Globally Applicable Approach. *Remote Sens.* **2018**, *10*, 1466. [CrossRef]
62. de Sousa, C.; Lagomasino, D.; Fatoyinbo, L. Mangroves II—Change Mapping. In *Cloud-Based Remote Sensing with Google Earth Engine*; Springer International Publishing: Cham, Switzerland, 2024; pp. 1045–1060, ISBN 9783031265877. [CrossRef]
63. Roy, D.P.; Kovalskyy, V.; Zhang, H.K.; Vermote, E.F.; Yan, L.; Kumar, S.S.; Egorov, A. Characterization of Landsat-7 to Landsat-8 Reflective Wavelength and Normalized Difference Vegetation Index Continuity. *Remote Sens. Environ.* **2016**, *185*, 57–70. [CrossRef]
64. Kennedy, R.E.; Yang, Z.; Cohen, W.B. Detecting Trends in Forest Disturbance and Recovery Using Yearly Landsat Time Series: 1. LandTrendr—Temporal Segmentation Algorithms. *Remote Sens. Environ.* **2010**, *114*, 2897–2910. [CrossRef]
65. de Jong, S.M.; Shen, Y.; de Vries, J.; Bijnaar, G.; van Maanen, B.; Augustinus, P.; Verweij, P. Mapping Mangrove Dynamics and Colonization Patterns at the Suriname Coast Using Historic Satellite Data and the LandTrendr Algorithm. *Int. J. Appl. Earth Obs. Geoinf.* **2021**, *97*, 102293. [CrossRef]
66. Xu, H. Modification of Normalised Difference Water Index (NDWI) to Enhance Open Water Features in Remotely Sensed Imagery. *Int. J. Remote Sens.* **2006**, *27*, 3025–3033. [CrossRef]
67. Xiao, X.; Boles, S.; Liu, J.; Zhuang, D.; Liu, M. Characterization of Forest Types in Northeastern China, Using Multi-Temporal SPOT-4 VEGETATION Sensor Data. *Remote Sens. Environ.* **2002**, *82*, 335–348. [CrossRef]
68. Huete, A. A Comparison of Vegetation Indices over a Global Set of TM Images for EOS-MODIS. *Remote Sens. Environ.* **1997**, *59*, 440–451. [CrossRef]
69. Ghorbanian, A.; Zaghian, S.; Asiyabi, R.M.; Amani, M.; Mohammadzadeh, A.; Jamali, S. Mangrove Ecosystem Mapping Using Sentinel-1 and Sentinel-2 Satellite Images and Random Forest Algorithm in Google Earth Engine. *Remote Sens.* **2021**, *13*, 2565. [CrossRef]
70. Diniz, C.; Cortinhas, L.; Nerino, G.; Rodrigues, J.; Sadeck, L.; Adami, M.; Souza-Filho, P.W.M. Brazilian Mangrove Status: Three Decades of Satellite Data Analysis. *Remote Sens.* **2019**, *11*, 808. [CrossRef]
71. Baloloy, A.B.; Blanco, A.C.; Raymund Rhommel, R.R.C.; Nadaoka, K. Development and Application of a New Mangrove Vegetation Index (MVI) for Rapid and Accurate Mangrove Mapping. *ISPRS J. Photogramm. Remote Sens.* **2020**, *166*, 95–117. [CrossRef]
72. Ligono, L.K.; Okolie, C.J. Integrated Analysis of Mangrove Changes Using the Mangrove Vegetation Index and Random Forest Classification in The Gambia. *ISPRS-Int. Arch. Photogramm. Remote Sens. Spat. Inf. Sci.* **2022**, *XLVI-M-2–2022*, 153–157. [CrossRef]
73. Li, H.; Han, Y.; Chen, J. Exploring the Capabilities of Combining the Sentinel-2 MSI Data and High Resolution Google Earth Image for Mapping Mangrove Species. In Proceedings of the IGARSS 2019—2019 IEEE International Geoscience and Remote Sensing Symposium, Yokohama, Japan, 28 July–2 August 2019; IEEE: Piscataway, NJ, USA, 2019; pp. 6879–6882.
74. Zhao, C.; Jia, M.; Zhang, R.; Wang, Z.; Ren, C.; Mao, D.; Wang, Y. Mangrove Species Mapping in Coastal China Using Synthesized Sentinel-2 High-Separability Images. *Remote Sens. Environ.* **2024**, *307*, 114151. [CrossRef]
75. Lombard, F.; Andrieu, J. Mapping Mangrove Zonation Changes in Senegal with Landsat Imagery Using an OBIA Approach Combined with Linear Spectral Unmixing. *Remote Sens.* **2021**, *13*, 1961. [CrossRef]
76. Zhang, T.; Hu, S.; He, Y.; You, S.; Yang, X.; Gan, Y.; Liu, A. A Fine-Scale Mangrove Map of China Derived from 2-Meter Resolution Satellite Observations and Field Data. *ISPRS Int. J. Geoinf.* **2021**, *10*, 92. [CrossRef]
77. Kint, A. De Luchtfoto En de Topografische Terresingesteldheid in de Mangrove. *Trop. Nat.* **1934**, *23*, 173–189. Available online: https://natuurtijdschriften.nl/pub/511106 (accessed on 30 January 2026).
78. Asbridge, E.; Lucas, R.; Ticehurst, C.; Bunting, P. Mangrove Response to Environmental Change in Australia's Gulf of Carpentaria. *Ecol. Evol.* **2016**, *6*, 3523–3539. [CrossRef]
79. Sidik, F.; Neil, D.; Lovelock, C.E. Effect of High Sedimentation Rates on Surface Sediment Dynamics and Mangrove Growth in the Porong River, Indonesia. *Mar. Pollut. Bull.* **2016**, *107*, 355–363. [CrossRef] [PubMed]
80. van Bijsterveldt, C.E.J.; van Wesenbeeck, B.K.; van der Wal, D.; Afiati, N.; Pribadi, R.; Brown, B.; Bouma, T.J. How to Restore Mangroves for Greenbelt Creation along Eroding Coasts with Abandoned Aquaculture Ponds. *Estuar. Coast. Shelf Sci.* **2020**, *235*, 106576. [CrossRef]
81. Castillo, Y.B.; Kim, K.; Kim, H.S. Thirty-Two Years of Mangrove Forest Land Cover Change in Parita Bay, Panama. *For. Sci. Technol.* **2021**, *17*, 67–79. [CrossRef]
82. Liu, T.; Huang, R.; Sun, Y.; Liu, Y.; Song, Z. Rapid Mangrove Expansion Triggered by Low River Discharge Episode in Nanliu River Estuary, Beibu Gulf of China. *Front. Mar. Sci.* **2024**, *11*, 1285518. [CrossRef]
83. Giri, C.; Long, J. Is the Geographic Range of Mangrove Forests in the Conterminous United States Really Expanding? *Sensors* **2016**, *16*, 2010. [CrossRef]
84. Visschers, L.L.B.; Santos, C.D.; Franco, A.M.A. Accelerated Migration of Mangroves Indicate Large-Scale Saltwater Intrusion in Amazon Coastal Wetlands. *Sci. Total Environ.* **2022**, *836*, 155679. [CrossRef]
85. Armitage, A.R.; Highfield, W.E.; Brody, S.D.; Louchouarn, P. The Contribution of Mangrove Expansion to Salt Marsh Loss on the Texas Gulf Coast. *PLoS ONE* **2015**, *10*, e0125404. [CrossRef]

86. Di Nitto, D.; Neukermans, G.; Koedam, N.; Defever, H.; Pattyn, F.; Kairo, J.G.; Dahdouh-Guebas, F. Mangroves Facing Climate Change: Landward Migration Potential in Response to Projected Scenarios of Sea Level Rise. *Biogeosciences* **2014**, *11*, 857–871. [CrossRef]
87. Cohen, M.C.L.; de Souza, A.V.; Rossetti, D.F.; Pessenda, L.C.R.; França, M.C. Decadal-Scale Dynamics of an Amazonian Mangrove Caused by Climate and Sea Level Changes: Inferences from Spatial-Temporal Analysis and Digital Elevation Models: Decadal-Scale Dynamics of an Amazonian Mangrove. *Earth Surf. Process.* **2018**, *43*, 2876–2888. [CrossRef]
88. Yang, S.-C.; Riddin, T.; Adams, J.B.; Shih, S.-S. Predicting the Spatial Distribution of Mangroves in a South African Estuary in Response to Sea Level Rise, Substrate Elevation Change and a Sea Storm Event. *J. Coast. Conserv.* **2014**, *18*, 459–469. [CrossRef]
89. Woodroffe, C.D. Response of mangrove shorelines to sea-level change. *Tropics* **1999**, *8*, 159–177. [CrossRef]
90. Ward, R.D.; de Lacerda, L.D. Responses of Mangrove Ecosystems to Sea Level Change. In *Dynamic Sedimentary Environments of Mangrove Coasts*; Elsevier: Amsterdam, The Netherlands, 2021; pp. 235–253. ISBN 9780128164372. [CrossRef]
91. Cohen, M.C.L.; Rodrigues, E.; Rocha, D.O.S.; Freitas, J.; Fontes, N.A.; Pessenda, L.C.R.; de Souza, A.V.; Gomes, V.L.P.; França, M.C.; Bonotto, D.M.; et al. Southward Migration of the Austral Limit of Mangroves in South America. *Catena* **2020**, *195*, 104775. [CrossRef]
92. Zhang, Z.; Ahmed, M.R.; Zhang, Q.; Li, Y.; Li, Y. Monitoring of 35-Year Mangrove Wetland Change Dynamics and Agents in the Sundarbans Using Temporal Consistency Checking. *Remote Sens.* **2023**, *15*, 625. [CrossRef]
93. Tran Thi, V.; Tien Thi Xuan, A.; Phan Nguyen, H.; Dahdouh-Guebas, F.; Koedam, N. Application of Remote Sensing and GIS for Detection of Long-Term Mangrove Shoreline Changes in Mui Ca Mau, Vietnam. *Biogeosciences* **2014**, *11*, 3781–3795. [CrossRef]
94. Suyarso, U.; Avianto, P. AMMI Automatic Mangrove Map and Index: Novelty for Efficiently Monitoring Mangrove Changes with the Case Study in Musi Delta, South Sumatra, Indonesia. *Int. J. For. Res.* **2022**, *2022*. [CrossRef]
95. Winarso, G.; Purwanto, A.D. Evaluation of Mangrove Damage Level Based on Landsat 8 Imagery. *Int. J. Remote Sens. Earth Sci. (IJReSES)* **2014**, *11*, 105–116. Available online: https://ejournal.brin.go.id/ijreses/article/view/14010 (accessed on 30 January 2026).
96. Rouse, J.W., Jr.; Haas, R.H.; Schell, J.A.; Deering, D.W. *Monitoring Vegetation Systems in the Great Plains with ERTS*; NASA: Washington, DC, USA, 1974; pp. 309–317. Available online: https://ntrs.nasa.gov/citations/19740022614 (accessed on 30 January 2026).
97. McFeeters, S.K. The Use of the Normalized Difference Water Index (NDWI) in the Delineation of Open Water Features. *Int. J. Remote Sens.* **1996**, *17*, 1425–1432. [CrossRef]
98. Gao, B.-C. NDWI—A Normalized Difference Water Index for Remote Sensing of Vegetation Liquid Water from Space. *Remote Sens. Environ.* **1996**, *58*, 257–266. [CrossRef]
99. Xiao, X. Modeling Gross Primary Production of Temperate Deciduous Broadleaf Forest Using Satellite Images and Climate Data. *Remote Sens. Environ.* **2004**, *91*, 256–270. [CrossRef]
100. Gitelson, A.A.; Viña, A.; Ciganda, V.; Rundquist, D.C.; Arkebauer, T.J. Remote Estimation of Canopy Chlorophyll Content in Crops. *Geophys. Res. Lett.* **2005**, *32*, L08403. [CrossRef]
101. Jordan, C.F. Derivation of Leaf-Area Index from Quality of Light on the Forest Floor. *Ecology* **1969**, *50*, 663–666. [CrossRef]